San Jose State University

SJSU ScholarWorks

2006

The effects of cold work and heat treatment on the properties of nitinol wire

Masao Jerome Drexel
San Jose State University

Follow this and additional works at: https://scholarworks.sjsu.edu/etd_theses

THE EFFECTS OF COLD WORK AND HEAT TREATMENT

ON THE PROPERTIES OF NITINOL WIRE

A Thesis

Presented to

The Faculty of the Department of Chemical and Materials Engineering

San Jose State University

In Partial Fulfillment

of the Requirements for the Degree

Master of Science

By

Masao Jerome Drexel

December 2006

UMI Number: 1441088

INFORMATION TO USERS

The quality of this reproduction is dependent upon the quality of the copy submitted. Broken or indistinct print, colored or poor quality illustrations and photographs, print bleed-through, substandard margins, and improper alignment can adversely affect reproduction.

In the unlikely event that the author did not send a complete manuscript and there are missing pages, these will be noted. Also, if unauthorized copyright material had to be removed, a note will indicate the deletion.

UMI®
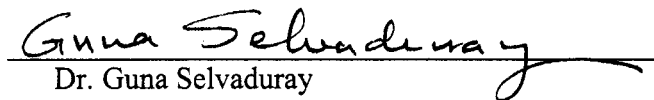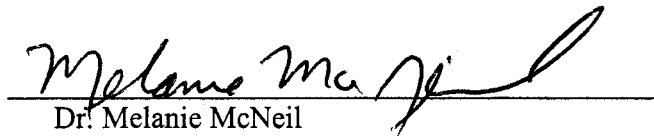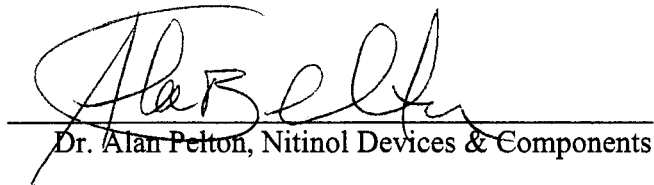
APPROVED FOR THE DEPARTMENT OF CHEMICAL

AND MATERIALS ENGINEERING

Guna Selvaduray

Dr. Guna Selvaduray

Melanie McNeil

Dr. Melanie McNeil

Alan Pelton

Dr. Alan Pelton, Nitinol Devices & Components

APPROVED FOR THE UNIVERSITY

Rhea I. Williamson 12/05/06

ABSTRACT

THE EFFECTS OF COLD WORK AND HEAT TREATMENT
ON THE PROPERTIES OF NITINOL WIRE

By Masao Drexel

The production of biomedical devices from Nitinol requires precise control of the

transformational and mechanical properties of the material. Heat treatments can be

utilized to tailor the properties and optimize performance. The effect of heat treatments

of 300 ~ 550°C for 2 ~ 180 minutes on Ti-50.8%Ni (at.%) wire of 30% and 50% cold

work was investigated. Transformational and mechanical properties were characterized

through the BFR method and tensile testing. Thermally activated precipitation and

annealing processes occurred. Annealing processes reduced the curvature and increased

the slope of BFR plots. The R-phase was present with greater frequency and prominence

in the 50% cold-worked wire than the 30% cold-worked wire. Two TTT diagrams were

constructed illustrating the trends in A_f of the wires. A maximum precipitation rate

occurred at approximately 450°C. The trends in UTS, UP, and LP are outlined for all

heat treatment conditions. Recrystallization began at 450°C for both wires.

ACKNOWLEDGMENTS

TABLE OF CONTENTS

LIST OF FIGURES

x

LIST OF TABLES

CHAPTER ONE
INTRODUCTION

1.1 History of Nitinol

The word Nitinol is an acronym for N̲ickel T̲itanium N̲aval O̲rdnance L̲aboratory. Nitinol refers to a family of near equiatomic nickel-titanium alloys[*]. The discovery of Nitinol, circa 1959, is credited to William J. Buehler. While working at the Naval Ordnance Laboratory, Buehler was investigating alloys of Ni and Ti as candidate materials for the nose cone of the U.S. Navy Polaris reentry vehicle. After melting Ni-Ti bars in an arc-casting furnace, Buehler routinely dropped them onto the concrete floor as a quick test of damping characteristics. To his surprise, Buehler noticed that a room temperature bar produced a dull "thud" sound. Disappointed, because he suspected that undesirable microcracks were the cause of the unexpected tone, Buehler dropped several more bars onto the floor. These bars, however, were still warm from the casting process and produced a high-pitched ringing sound. Surprised by the difference, Buehler heated and cooled the Ni-Ti bars several times and found that the acoustical changes were reproducible. After assuring himself that the bars were all of the same composition, he theorized that the change in the acoustical properties of the alloy must be linked to a low temperature atomic rearrangement. Although his discovery was never useful in the Polaris project, Buehler continued to research this interesting material. Through further experimentation and research of Nitinol, by Buehler as well as others, an understanding

---

[*] The term alloy is used here loosely, to describe a combination of two metallic elements. Strictly speaking, Nitinol is an ordered intermetallic compound, or "line" compound, because it has 1:1 Ni:Ti stoichiometry.

of the near room temperature phase transformation – atomic rearrangement – was eventually developed [1].

Initially, Nitinol received little attention outside of research laboratories because of its unconventional properties. Design engineers were unsure how to utilize the unique attributes and as yet unexplored potential of Nitinol. The fact that the properties of Nitinol change significantly with small variations in composition and temperature further complicated the understanding and integration into the market place of Nitinol. With time, researchers began to focus on specific alloy compositions, which provide reproducible properties. Eventually designers found niche applications where the special properties of Nitinol could be exploited.

1.2 Applications of Nitinol

In 1969, the first successful application of Nitinol occurred as a pipe coupler in the U.S. Navy F-14 jet fighter [1]. Nitinol couplers were, and still are, used in these jets to connect discontinuous metal tubing in the high-pressure hydraulic fluid system. As a coupler material a tubular section of Nitinol is first machined from barstock. The tube is then cooled to a temperature sufficient to stabilize the low temperature phase. While cool the tubular section is expanded to allow the insertion of the two pipes to be joined. As the Nitinol coupler warms the phase transformation between low and high temperature phases causes the coupler to shrink – forming a tight seal around the two pipes. Marine couplers have since been developed and couplers continue to be one of the successful applications of Nitinol.

The discovery of the good biocompatibility of Nitinol, due to the rapid formation of a passive titanium oxide surface layer, has led to the wide spread application of Nitinol in the biomedical industry [2]. Nitinol is utilized in the field of endovascular medicine as a stent[†] material. Although 316L stainless steel is still the most common material used for stents, Nitinol stents are preferred in superficial regions of the body, such as the carotid and femoral arteries. The superior springback capabilities of Nitinol make it well suited for these vulnerable locations. A superficial impact can cause a stent to become partially or even completely compressed within the body. This impact will cause a Nitinol stent to change its atomic arrangement – change phase. After impact, a Nitinol stent can completely recover its original shape due to the reverse phase transformation. Stainless steel stents, on the other hand, have limited ability to recover from a crushing impact, which can lead to a reduction in blood flow and increased morbidity. The high level of strain that is recoverable by a Nitinol stent is shown in Figure 1.

(a)   (b)
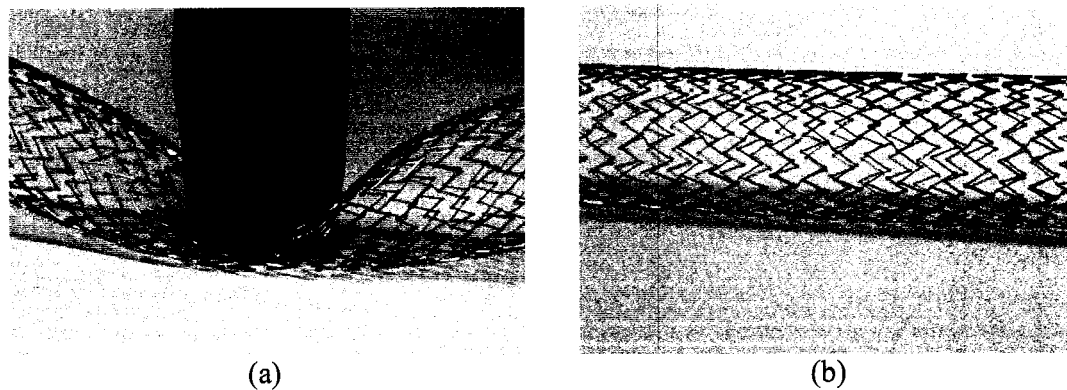
Figure 1. A compressed Nitinol stent, (a), will completely recover its original shape, (b).

[†] Stent - a cylindrical metal scaffold implanted to stabilize and prop open a vein or artery, often following a balloon angioplasty procedure.

The introduction of Nitinol to dentistry in 1988 has "revolutionized" the root

canal procedure, according to Dr. John H. Newman [3-4]. In the field of endodontics,

Nitinol is utilized, with great success, as the functional material for endodontic files.

These files are used during root canal procedures to clean and expand the curved tooth

canal where the nerve was previously housed. Prior to the introduction of Nitinol files,

curved stainless steel hand files were used. The stainless steel files had to be maneuvered

slowly and with exceptional care in order to avoid breaking them inside the tooth canal.

Nitinol files, because of their superelastic behavior, can conform to the shape of the root

canal without breaking. In addition the superior kink resistance of Nitinol permits the use

of a rotary drill to power the files. This eliminates the tedious and potentially

problematic hand filling process required by stainless steel files. The superior elastic

deformation permitted by Nitinol endodontic files is shown in Figure 2.

Applications such as pipe couplers, stents and endodontic files all require precise

control of the properties of Nitinol. Similar to conventional metals, the mechanical

(a)   (b)
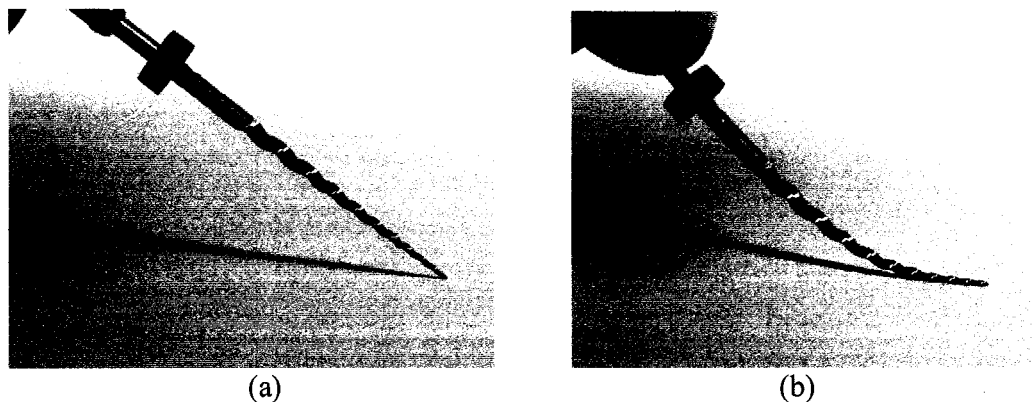
Figure 2. Endodontic file, (a), under elastic deformation sufficient to conform to a tooth
canal, (b).

properties of Nitinol can be modified during processing. Deforming the material can strengthen it while annealing treatments can be used to increase ductility and workability. Unlike conventional metals, however, the performance of Nitinol also depends on the materials transformational properties. For example, a "self-expanding" stent will deploy within the body when heated above its transformation temperature. Therefore, the transformational properties of Nitinol must also be monitored and controlled during processing. The effects of cold work, heat treatment temperature, and heat treatment time on both the mechanical and transformational properties of Nitinol were investigated in this study.

In Chapter Two a more detailed explanation of the phase transformation and its relationship to the unique properties of Nitinol is given. Also, a brief overview of cold work and the potential effects on the aging response are presented. The specific objectives of this study are explained in Chapter Three. The experimental materials, equipment, and methods used are discussed in Chapter Four. The results are presented and discussed in Chapters Five and Six, respectively. Conclusions drawn from this research follow in Chapter Seven. Recommendations for future work are contained in Chapter Eight.

CHAPTER TWO

LITERATURE REVIEW

2.1 Background

Buehler's discovery of the difference in damping characteristics between warm

and room temperature Nitinol bars when dropped on the floor, indicated to him that a

change in the internal structure of the metal must have occurred. Although Buehler did

not know the details of the curious behavior of Nitinol at the time, his postulation was

correct. It is now known that the unique properties of Nitinol are the result of a near

room temperature solid-state phase transformation. When heated to temperatures above

the transformation temperature, Nitinol exists in the austenite or "parent" phase. In the

austenite phase, Nitinol possesses the B2 CsCl crystal structure. When cooled below the

transformation temperature, Nitinol exists in the martensite phase with the B19'

monoclinic crystal structure. The transformation between the high and low temperature

phases of Nitinol is "martensitic" in nature, meaning that no atomic diffusion occurs.

This has to be the case because the transformation temperatures are not sufficiently high

to permit significant atomic mobility. Instead, the transformation involves a shear-like

motion of the atomic planes in which atomic correspondence between neighboring atoms

is maintained and no bonds are broken or formed. The temperature at which this phase

transformation takes place is a function of both composition and processing history.

A generic heating and cooling path for Nitinol under a constant load is shown in

Figure 3. Two temperatures are defined on the cooling path: M_s is the martensite start

temperature, where transformation from austenite to martensite begins, and M_f is the

martensite finish temperature, where the transformation completes and the material exists in the low temperature martensite phase. On the cooling path, the A_s, austenite start temperature, and the A_f, austenite finish temperature, are similarly defined for the transformation from martensite to austenite.

The change in length associated with the austenite-martensite transformation, seen in Figure 3, illustrates the significant change in mechanical properties resulting from the phase transformation. Under constant load, a Nitinol specimen will lengthen when cooled to martensite as a result of a decrease in stiffness. Conversely, if the Nitinol specimen is heated until austenite is stabilized, it will shorten as a result of an increase in stiffness [5,6]. The austenite-martensite transformation is referred to as "thermoelastic" because it can be induced through temperature change or mechanical strain.

The stress-induced transformation from austenite-to-martensite clearly distinguishes the stress-strain response of Nitinol from that of a conventional engineering alloy, such as stainless steel. A comparison between the deformation responses of
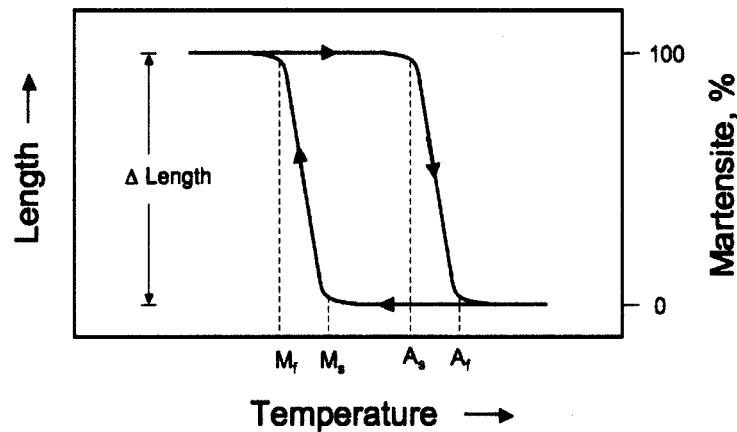
Figure 3. Heating and cooling paths for Nitinol wire under a constant load [5].

7

Nitinol and stainless steel is shown in Figure 4. During loading, a stainless steel specimen will deform elastically until the yield strength is reached, which in Figure 4 (a) occurs at a stress of 660 MPa and a strain of approximately 0.5%. After yielding, stainless steel will deform plastically, *i.e.*, in a non-recoverable manner, until the ultimate tensile strength (UTS) of the material is reached, followed by failure when the fracture stress is reached. Nitinol on the other hand, if processed correctly, can change phase upon loading producing a "loading plateau" in the stress-strain diagram, shown in Figure 4 (b). This loading plateau resides between the linear elastic deformation regions of the initial austenite and stress-induced martensite phases. Because of this austenite-to-martensite phase transformation, the critical strain for plastic deformation is over one order of magnitude larger in Nitinol than in stainless steel, in Figure 4 (b) yielding occurs at a strain of approximately 10%. It should be noted that the processing conditions of the two materials represented in Figure 4 are not the same, therefore the differences in the UTS and yield strength values resulted from both material and processing differences.
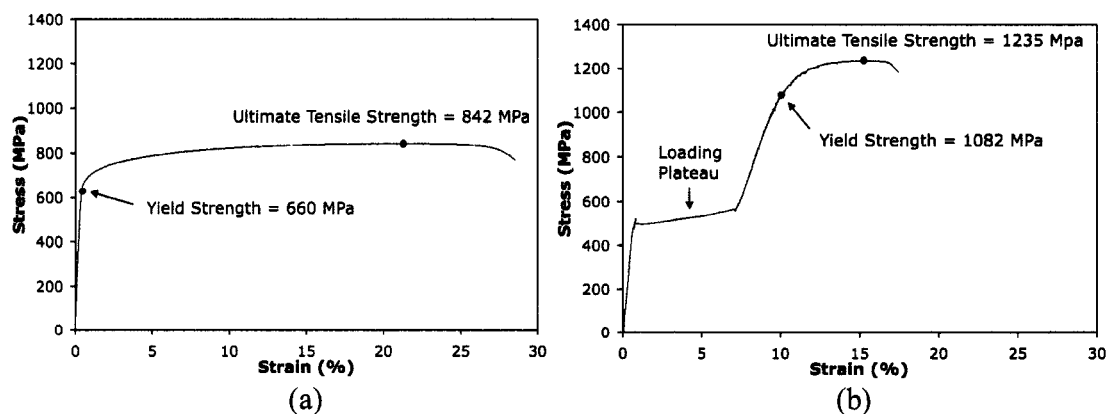
Figure 4. The tensile responses of (a) stainless steel and (b) Nitinol.

Inducing a phase transformation, however, is not assured when loading Nitinol.

The transformation temperature and test temperature will both factor in to determine the

material response. The stress-strain response of Nitinol in three different temperature

regimes is shown in Figure 5. When Nitinol is in the austenite phase, *i.e.*, at a

temperature above A_f, and at a temperature below the martensite deformation temperature

(M_d), an applied stress will initially cause linear elastic deformation as the result of bond

stretching – similar to conventional metals. But, when a critical stress is reached, the

alloy will begin transformation to the martensite phase to accommodate the strain. The

beginning of this transformation is seen as point A. With continued loading, the

martensite phase will grow at the expense of the austenite phase, until eventually the

austenite-to-martensite transformation is complete at point B. If loading continues,
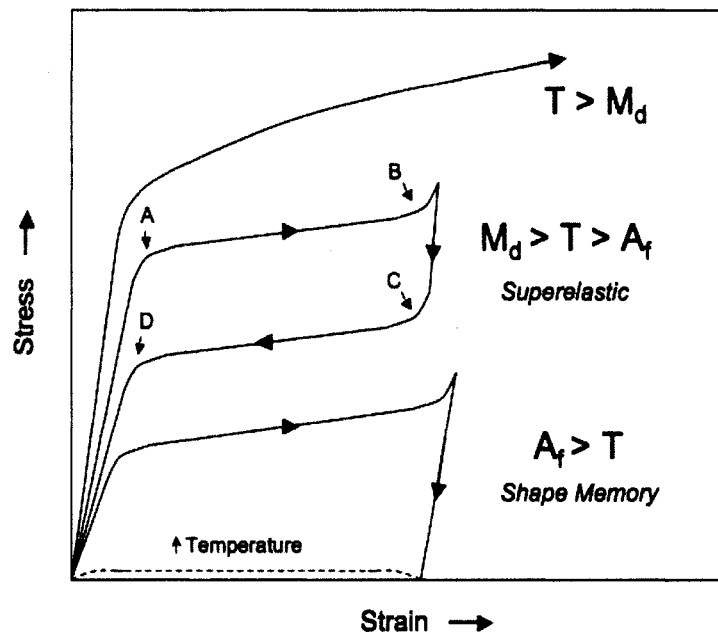
Figure 5. The Nitinol stress-strain responses for three temperature regimes [5].

elastic deformation of the martensite phase will occur, followed by plastic deformation as was shown previously in Figure 4 (b). If the specimen is unloaded from point B, another critical stress will be reached where the reverse transformation from martensite-to-austenite begins at point C. With continued unloading the martensite phase will be consumed until the reverse transformation from martensite-to-austenite is complete at point D. Finally, complete unloading will result in the elastic recovery of the austenite phase. This type of elastic deformation has been named "superelastic" because strains of up to approximately 8% can be completely recovered [7]. For comparison, stainless steels are typically capable of recovering elastic strains of only 0.8% or less. Superelastic behavior is also referred to as "pseudoelastic" because, unlike conventional linear elastic behavior, which results from the stretching of atomic bonds, superelastic behavior is non-linear and results primarily from a phase transformation.

The martensite deformation temperature, M_d, is the temperature above which the austenite-to-martensite phase transformation can no longer be stress induced. If Nitinol is deformed at temperatures above M_d, the material will behave as a conventional metal; the stress-strain curve will display linear elasticity until a yield point is reached where plastic deformation will begin and eventually the UTS will be reached.

If Nitinol is sufficiently deformed at a temperature below A_f, any existing austenite will transform to martensite. As in superelasticity, increasing the stress will tend to increase the amount of martensite. Unlike superelasticity, however, during unloading, the thermal energy will not be sufficient to drive the reverse reaction and the Nitinol will remain as martensite. If sufficient thermal energy is supplied to heat the

Nitinol above A_f, the transformation back to austenite will occur and the strain will be recovered. This recovery of strain through heating is referred to as the "shape memory effect". The capability of Nitinol to recover a preset shape through heating, places it in a class of materials referred to as shape memory alloys (SMAs) [6].

2.2 Compositional Effects

The austenite-martensite transformation temperature of Nitinol changes with composition. Melton has collected data from several researchers showing the differences in M_s for a range of Nitinol compositions [8]. The M_s values reported by these researchers do not agree perfectly because the variety of techniques that were employed influenced the results. For example, the data measured by Wang $et\ al.$ utilized the sound from hitting heated specimen as a means of measuring the transformation temperature [9]. This technique is clearly qualitative and the data must be considered accordingly. Ignoring the small variations in the data presented by Melton, a general trend is supported by all the data, showing an increase in transformation temperature with increased Ti concentration. The plot of M_s versus composition published by Melton, without the data of Wang, is shown in Figure 6. The M_s temperature is seen to change from approximately 50°C for an alloy of Ti-50%Ni (at.%) to approximately -100°C for an alloy of Ti-51%Ni (at.%). Ni-rich Nitinol alloys are commonly processed with a target composition of approximately 51%Ni (at.%) [10].

The ability to adjust the austenite-martensite transformation temperature of Nitinol through changing the material composition is very useful. In biomedical

11
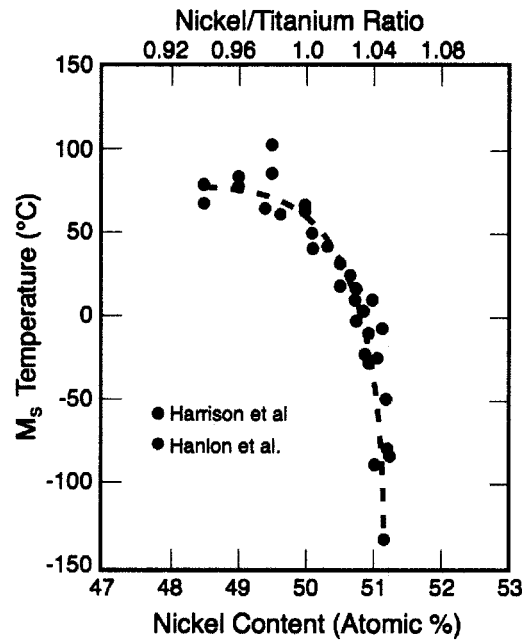
Figure 6. Trend in M_s as a function of composition [8].

applications this capability is sometimes utilized for device deployment. For example,

Nitinol stents can be processed to have a transformation temperature slightly below body

temperature. Prior to surgery, the stent is cooled to at temperature below the

transformation temperature of the material, stabilizing the martensite phase. As

martensite, the stent is easily crimped to a diameter small enough to allow insertion into

the body. Once deployed inside the targeted vein or artery the stent is warmed by body

heat, causing transformation to the high temperature austenite phase, which results in

expansion of the stent due to the shape memory effect. By the time the stent reaches

body temperature it will have completely expanded to the desired operating diameter.

Obtaining Nitinol with a specific transformation temperature requires

compositional tolerances of between one tenth and one hundredth of a percent [8]. These

tolerances are beyond common metallurgical practices and therefore the transformation temperature cannot be easily set by metallurgy alone. The application of Nitinol requires the setting of precise and reproducible transformation temperatures, especially in the biomedical industry where the tolerances are strict and specific.

2.3 Precipitation Processes in Nitinol

Fortunately, the tight composition tolerances required for obtaining a desired transformation temperature are not placed solely on metallurgical practices. This is because, through heat treatment, the precipitation of non-equiatomic phases can be utilized to gradually alter the surrounding matrix composition, thereby changing the transformation temperature. In this way, different transformation temperatures can be tailored for specific applications from a single starting composition.

The precipitation processes of Ti-52%Ni and Ti-50%Ni (at.%) materials have been researched in depth by Nishida et al. and Saburi [11,12]. Nishida has constructed a Time-Temperature-Transformation (TTT) diagram that illustrates the formation of a series of Ni-rich precipitates over a range of heat treatment temperatures and times. In the temperature range below $680 \pm 10°C$ the precipitation process is:

$$\beta_0 \rightarrow \beta_1 + Ni_4Ti_3 \rightarrow \beta_2 + Ni_3Ti_2 \rightarrow \beta_3 + Ni_3Ti \qquad \text{Equation 1}$$
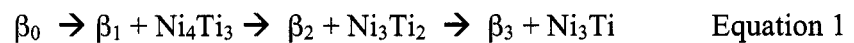
where β_0 is the initial matrix composition, β_1 is the matrix composition in equilibrium with Ni_4Ti_3 and so on. The final NiTi and Ni_3Ti phases are the stable equilibrium phases of the Nitinol phase diagram. The Ti_3Ni_4 and Ni_3Ti_2 phases are metastable and form in the order of increasing Ni content. This precipitation sequence depletes nickel from the

surrounding matrix resulting in an increase in the martensite-austenite transformation temperature. A change in M_s of 150°C has been reported by Melton through aging Ti-51.5%Ni (at.%) at 400°C [8].

Pelton *et al.* have outlined another form of TTT diagram that illustrates the trend in A_f as a function of time and temperature for Ti-50.8%Ni (at.%), shown in Figure 7 [13]. Two "noses" are apparent in the TTT diagram, which indicate the locations of maximum increase in A_f during heat treatment. The larger nose is positioned at 450°C and a smaller nose at about 575°C. These two noses result from the nucleation and growth processes of the Ni-rich precipitates.

At high temperatures, the precipitate growth rate is increased by greater atomic mobility. However, the critical size of a stable nucleus is large, resulting in a low
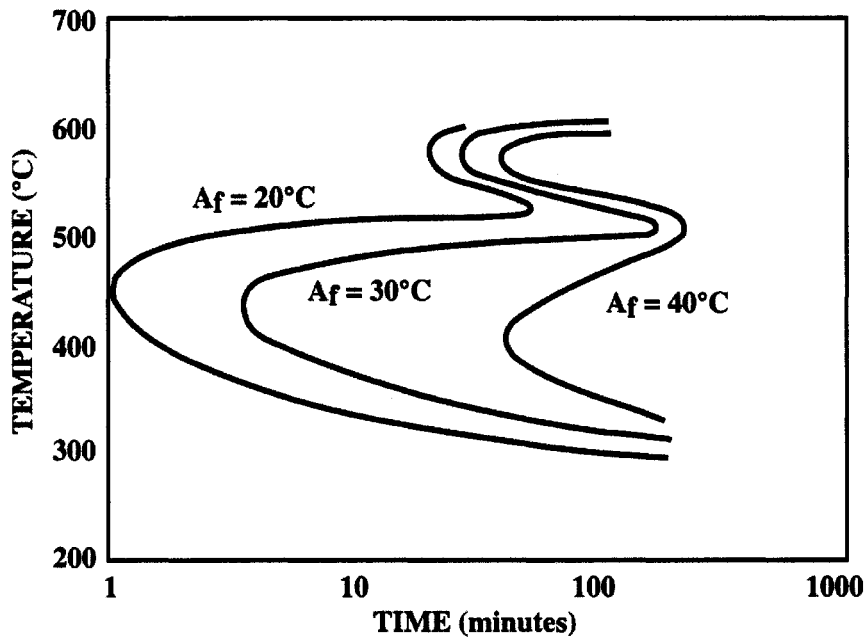
Figure 7. TTT diagram showing the A_f increase during heat treatment [13].

nucleation rate. At lower temperatures, the driving force for nucleation is higher and the critical size nucleus is smaller but the atomic mobility is low, leading to slow growth rates. The maximum precipitation rate, therefore, occurs at an intermediate temperature where a balance between nucleation and growth rates is obtained. The large maximum, at 450°C, corresponds to the highest rate of precipitation of Ni_4Ti_3 and the smaller, 575°C, maximum is attributed to the highest rate of precipitation of Ni_3Ti_2. Interestingly, during aging at 550°C an initial decrease in A_f occurred prior to the expected increase. This decrease is attributed to dissolution of the Ni_4Ti_3 precipitate, which increases the nickel content of the matrix, prior to the eventual formation of Ni_3Ti_2 and Ni_3Ti [13].

2.4 Cold Work and Recovery Processes

Nitinol is commonly available in a variety of physical forms including sheet, tube, and wire. To achieve these geometries, a series of hot and cold working processes are utilized. Typical levels of cold work[‡] for processed Nitinol wire and tubing fall into the range of 30 ~ 50%. Cold working metals results in an increase in their defect density. The concentration of vacancies, interstitials, and dislocations all increase in metals during cold work. Dislocation densities have been reported to increase four to six orders of magnitude during heavy cold working of metals [14]. A fraction of the energy input during cold work is stored as elastic strain energy inside the deformed metal. This strain energy will act to impede further dislocation motion in the metal, resulting in an increase in the UTS and a decrease in the maximum elongation.

[‡] Cold Work: deformation at temperatures where annealing does not occur; calculated as the percent reduction in the cross-sectional area.

It has been reported by Aaronson that, in some alloys, dislocations act as catalysts for the nucleation process by reducing the strain energy required to form a critical size nucleus [15]. An increase in the nucleation rate of the Ni-rich precipitates as a result of cold work in Nitinol would be expected to shift the constant A_f curves in the TTT diagram constructed by Pelton up and to the left. A shift up would result because higher nucleation rates act to decrease the amount of under-cooling required to "drive" the nucleation process. A shift to the left would result from the increased number of nuclei creating a more rapid change in the matrix composition during precipitation.

If accelerated nucleation rates result from a high dislocation density, the processes of annealing will diminish this effect. Annealing processes consist of recovery, recrystallization, and grain growth. Recovery occurs when a cold-worked metal is provided thermal energy sufficient to activate a reduction in the lattice strains through the rearrangement and elimination of defects. Recovery processes can be separated into two regimes: low and high temperatures. Low temperature recovery involves a reduction in the number of point defects to their equilibrium values. High temperature recovery processes include the rearrangement and annihilation of dislocations. Dislocation stresses are reduced through polygonization. During polygonization, dislocations rearrange themselves into subboundaries[§]. The formation of rearranged dislocation structures reduces the total stored internal energy of the metal and is therefore an energetically favorable process. Dislocation annihilation occurs when neighboring dislocations combine and, literally, annihilate one another. The result of dislocation

---

[§] Subboundaries: ordered dislocation structures that separate regions of a grain.

annihilation is a reduction in the stored internal energy and a decrease in dislocation density [15]. A study preformed by Pelton *et al.* has shown that recovery processes can occur in cold-worked Nitinol at 500°C in as little as 5 minutes [13].

Recrystallization occurs when sufficient thermal energy is provided for the nucleation and growth of new strain-free grains. The recrystallization process will proceed until the new grains impinge on one another and all of the original cold-worked grains have been consumed. Similar to recovery, this process decreases the total internal energy of the metal and is energetically favorable. A critical temperature must be reached before recrystallization will occur. Stored internal energy introduced during cold work facilitates the recrystallization process by lowering the activation energy required for recrystallization [15]. A higher level of cold work will therefore lead to a lower recrystallization temperature. A study preformed by Saburi has documented the recrystallization of 25% cold-worked Nitinol at 600°C after heat treatment for one hour [12]. Miyazaki, in another study, has documented recrystallization of cold-worked Nitinol after heat treatment at 500°C for one hour; the extent of the cold work was not identified [16].

2.5 Literature Review Summary

Beginning with the discovery of Nitinol in 1959, an understanding of the material has been developed through the contributions of many scientists over the last half-decade. Many of the mysteries of this unique material have been solved, including the mechanisms of the shape memory effect and superelasticity. The austenite-martensite

17

phase transformation has been investigated on a microscopic level and explained in detail. Through the discovery of the relationship between composition and transformation temperature a method of controlling the transformational properties has been developed. The ability to modify the matrix composition through the precipitation of Ni-rich phases during heat treatment has provided the means by which devices with consistent transformational properties can be produced. Recent research has focused on more subtle aspects of the behavior of the material, such as the effects of temperature and time on the precipitation reactions. To this end, the study by Pelton *et al.* has presented a TTT diagram that illustrates the changes in A_f during heat treatment at a range of relevant times and temperatures. This research takes one further step by investigating the effect of the level of initial cold work on the TTT diagram for A_f temperatures.

CHAPTER THREE
RESEARCH OBJECTIVES

The objective of this study was to characterize the trends in the thermal and mechanical properties of 30% and 50% cold-worked Nitinol wire during heat treatment at 300 ~ 500°C for 2 ~ 180 minutes. Previous studies have examined the precipitation sequence of Ni-rich Nitinol in depth and current industry practices utilize heat treatment as a means of carefully adjusting the matrix Ni-Ti ratio. The recent study by Pelton *et al.* has examined the precipitation reactions from a metallurgical perspective, outlining the TTT diagram shown in Figure 4 [13]. This study provides insight into the effects of time and temperature on the precipitation reactions. However, the wire utilized in Pelton's study was thermally straightened, after drawing to approximately 40% cold work, effectively reducing the extent of cold work in the material. The present research sought to expand upon Pelton's research by starting with Nitinol wire with two levels of cold work – 30% and 50%. These levels of cold work were selected because current Nitinol processing typically yields material with cold work in the range of 30 ~ 50%. Therefore, this study examined the response of Nitinol wire to heat treatment at the limits of the common range of as-drawn cold work.

Most biomedical devices place demands on both the mechanical and transformational properties of Nitinol. Therefore, the effects of cold work, heat treatment temperature, and heat treatment time on both the mechanical and transformational properties of the wire were studied.

19

CHAPTER FOUR

MATERIALS AND METHODS

The experimental materials, methods, and results of this study are summarized in

Figure 8. Starting wire was processed to obtain wires with nominal 30% and 50% cold

work. The cold-worked wires were then heat-treated at 300 ~ 550°C for 2 ~ 180 minutes.

As-drawn and heat-treated wires were tested with the Bend and Free Recovery (BFR)

method and in uniaxial tension to characterize their transformational and mechanical

properties, respectively. A Scanning Electron Microscope (SEM) equipped with an
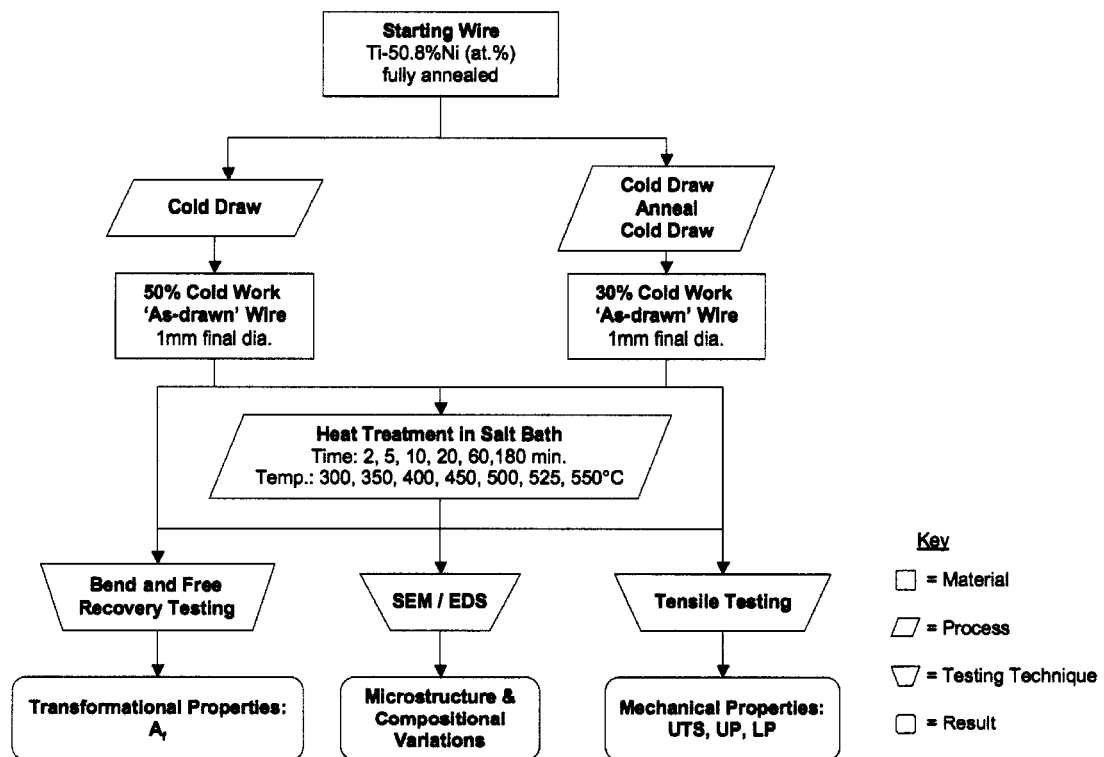
Figure 8. Experimental flow diagram.

Energy Dispersive X-ray Spectroscopy (EDS) detector was used to investigate the microstructure of the wires and the relative composition of the detected phases. A detailed explanation of the materials and methods is contained in the following sections: 4.1 Materials, 4.2 Equipment, and 4.3 Experimental Approach.

4.1 Materials

Both of the Nitinol wires studied originated from the same ingot, which was purchased by Nitinol Devices and Components (NDC) from Wah Chang. The Nitinol wires were drawn at NDC to a 1 mm final diameter after 30.4% and 50.7% cold work. These wires are referred to as having 30% and 50% cold work throughout this thesis. The composition of both wires used in this study was Ti-50.8%Ni (at.%) with trace amounts of oxygen, iron, and carbon impurities. The wires used in this study meet the high compositional requirements dictated by the biomedical industry. The composition of the wires is provided in Table 1 [17].

Table 1. Nitinol Wire Composition.

Ni (wt.%)	Ti	Fe (wt.%)	C (wt.%)	O (wt.%)	H (wt.%)
55.9	Balance	0.010	0.0031	0.034	< 0.002

The 30% and 50% cold-worked wires were drawn from the same parent lot. Cold work was introduced to the wires through a series of cold drawing steps. The parent lot was fully annealed prior to cold drawing. A second full anneal was performed on the

30% cold-worked wire prior to the final cold drawing steps used to obtain the desired level of cold work. The 50% cold-worked wire was drawn directly to its final diameter.

4.2 Equipment

4 mm inner diameter Nitinol tubing was used to house and straighten the wires during heat treatments performed at NDC in salt pots, which consisted of a metal bath surrounded by insulation and heating elements. The bath volume was approximately 4 liters. Blue Temp Salt # 275, which consists of a fifty-fifty mixture of sodium nitrite and potassium nitrite, was used in the baths. The melting temperature of the salt is 280°C and the pots were calibrated through a maximum temperature of 575°C. Type K thermocouples of 1/8-inch diameter were used to monitor the salt bath temperatures. Micro Precision, Inc calibrated all the salt pots and thermocouples used in this study. The wires, still housed in tubing, were quenched in a water bath after heat treatment.

Schematic illustrations of the mandrel and the BFR test apparatus utilized are shown in Figures 9 and 10, respectively. A 49 mm diameter circular mandrel, consistent with the American Society of Testing Materials (ASTM) standard F2082-03, was used to
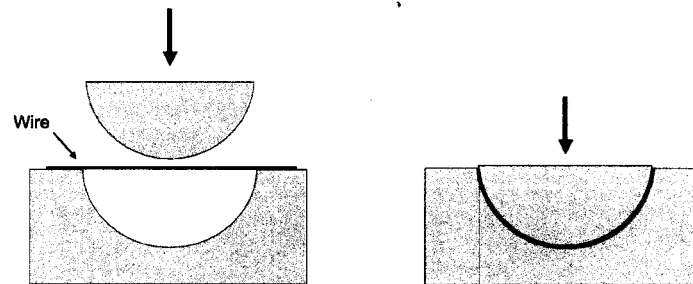
Figure 9. BFR test mandrel.
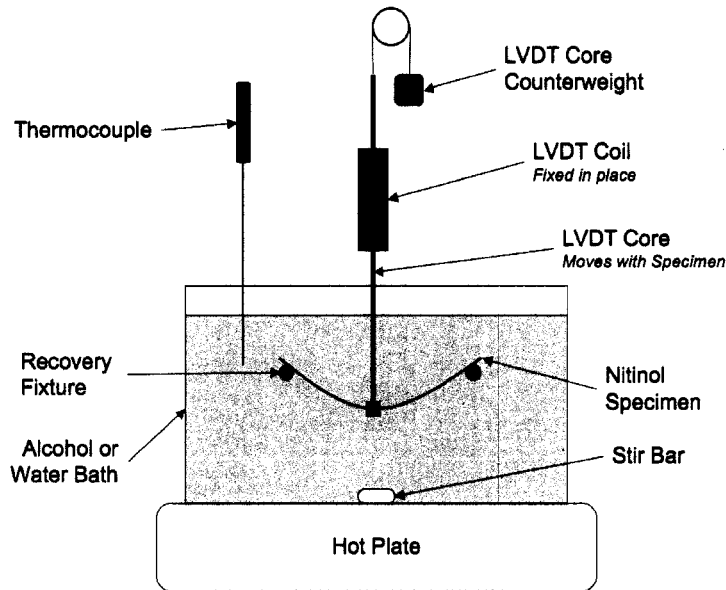
Figure 10. BFR test apparatus.

strain the wires between 2% and 2.5% during BFR testing [18]. The BFR apparatus

shown in Figure 10 included a liquid bath placed on a hot plate for heating. The

"recovery fixture" supported the wire specimens during testing. A stir bar was used to

assure thermal equilibrium between the bath and the wire specimens. The displacement

of the wires, as the bath was heated, were monitored with a linear variable displacement

transducer[**] (LVDT). A counterweight attached to the LVDT core reduced the

downward force on the wire specimens to less than 5 g. The bath temperature was

monitored by a type T thermocouple also calibrated by Micro Precision, Inc.

Uniaxial tensile testing was performed with an Instron 55R1123 tensile tester

equipped with pneumatic grips and a 450 lb load cell. Strain was measured with a clip-

---

[**] An LVDT consists of a magnetic iron core that travels through a set of stationary coils. As the core moves, a voltage is created in the coils proportional to the displacement.

on extensometer. The load cell and extensometer were both calibrated by Instron. Sandpaper was placed on the grip faces and the grip pressure was adjusted to reduce grip-initiated failures.

SEM analysis was performed at both NDC and BAE Systems. A JEOL JSM 5600 SEM was used at NDC to image the microstructure of the wires. A FEI Quanta 600 SEM equipped with an Oxford EDS detector and INCA System software was used at BAE Systems to investigate the relative compositions of the phases. Contrast between the phases was obtained through the detection of backscattered electrons. The INCA software "point and ID" mode was used to determine the relative compositions of the phases. All SEM specimens were mounted and polished prior to analysis.

4.3 Experimental Approach

Salt pots were chosen to heat-treat the wires because of the fast heating rates resulting from the high thermal conduction between the liquid salt and the Nitinol. Rapid heating and cooling rates are preferred so that heat treatment times have a higher degree of accuracy. This is especially important for short heat treatments, where heat up times can constitute a significant portion of the total heat treatment time. The post heat treatment water quench was utilized to reduce the cool down times.

Heat treatments with dwell temperatures of 300, 350, 400, 450, 500, 525, and 550°C for 2, 5, 10, 20, 60, and 180 minutes were performed on both 30% and 50% cold-worked wires. Small time intervals were used between the shorter heat treatment times to capture the rapid initial changes in A_f previously reported by Pelton et al. [13]. The

seven heat treatment temperatures were chosen to accurately outline the anticipated lower

nose of the TTT diagram published by Pelton, which was shown in Figure 7. The

temperature of 525°C was added to capture the cusps in the two precipitation noses

illustrated by the diagram. Table 2 is a summary of the heat treatment conditions.

Table 2. Heat Treatment Conditions.

Cold Work Conditions (%)	Heat Treatment Temperatures (°C)	Heat Treatment Times (min.)
30, 50	300, 350, 400, 450, 500, 525, 550	2, 5, 10, 20, 60, 180

A_f values of the Nitinol wire were determined with the BFR method in

accordance with ASTM F2082-03 [18]. The BFR technique involves cooling the Nitinol

specimens sufficiently to stabilize their martensite phase, $i.e.$, to a temperature below M_f.

Specimens that required cooling below room temperature were placed into chilled

alcohol baths. Bath temperatures down to -70°C were usually sufficient to stabilize the

martensite phase for the materials in this study. When cooling below room temperature

was not required, a room temperature water bath was used. While martensitic, and still

submerged in the bath, a strain of 2 ~ 2.5% was applied to the wire specimens by

manually forcing them to conform to the circumference of the 49 mm diameter circular

mandrel, which was shown in Figure 9.

After the cooled Nitinol wire was strained, it was moved from the mandrel into

the BFR apparatus. A schematic diagram of the BFR test apparatus was previously

shown in Figure 10. The wire was not removed from the cold liquid bath between

deformation and testing to ensure maintenance of the martensite phase. Next, the alcohol or water bath was heated on a hot plate at a rate of no more than 4°C/min. The slow heating rate and a stir bar were used to assure constant thermal equilibrium between the bath and wire. As the wire was heated, it slowly recovered its original unstrained shape as a result of the shape memory effect. During testing the temperature and displacement data acquired from the thermocouple and LVDT, respectively, were combined to construct the BFR plots. A sample BFR plot is shown in Figure 11.

The A_f temperatures of the wires were extracted from the collected BFR plots. The ASTM standard requires the use of two tangent lines when determining the A_f of the specimens. This method is sufficient in fully annealed samples where little cold work
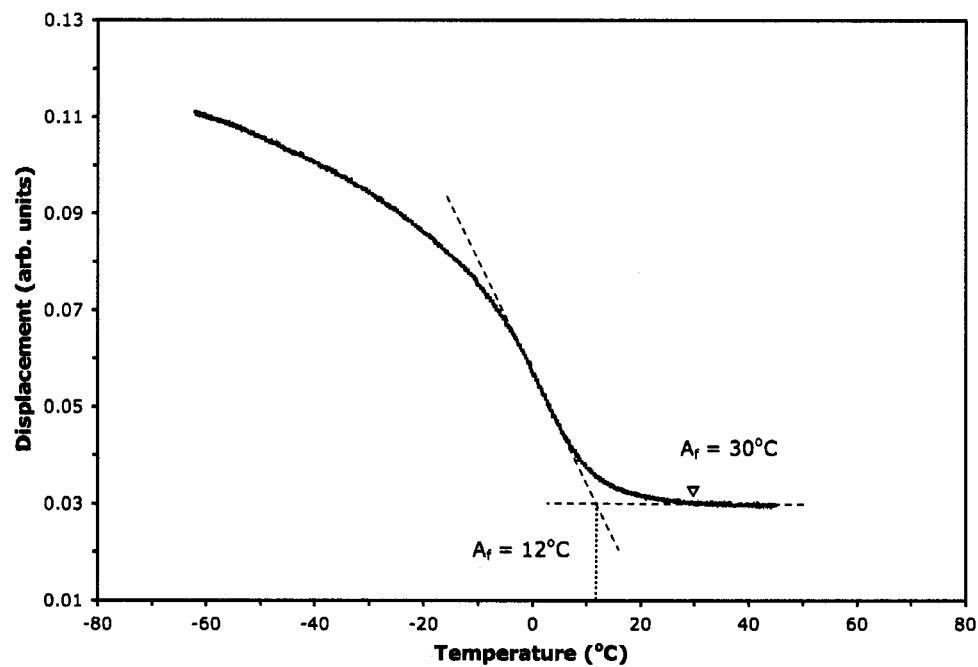
Figure 11. BFR plot of heavily cold-worked Nitinol.

26

remains. In this study, however, there were high levels of cold work remaining in many of the specimens, which resulted in BFR plots with significant amounts of curvature. Therefore, determination of the A_f through the use of the tangent intersection method would have resulted in A_f values that did not corresponded to the end of displacement, *i.e.*, the end of the phase transformation. A 28°C difference between the A_f values determined by tangent lines and by the end of displacement is shown in Figure 11. In this study the A_f was identified as the point at which recovery ended. It should be noted that this method of determining the A_f is problematic as well, because there is a level of speculation when defining the end of displacement. To increase the consistency in A_f determination, tangent lines were fit to the lower, flat, portions of the BFR curves. This helped when selecting the temperature where displacement ceased – the A_f temperature.

For some cold work and heat treatment conditions the transformation from martensite-to-austenite will occur via a third intermediate phase, called the rhombohedral phase, or "R-phase", which is discussed in more detail in Section 5.2. When the R-phase is stabilized the transformation is referred to as a two-stage transformation. Upon heating, two-stage transformations proceed sequentially: martensite – R-phase – austenite. In this case ASTM recommends determining the A_f through the tangent line technique illustrated in Figure 12. ASTM does not, however, address cases where the second step is subtle. When the second step in a two-stage transformation is subtle determining if a two-stage transformation has occurred is not trivial, as was the case for many of the heat treatment conditions in this study. During this study the A_f was determined with the same technique for both one and two-stage transformations – the
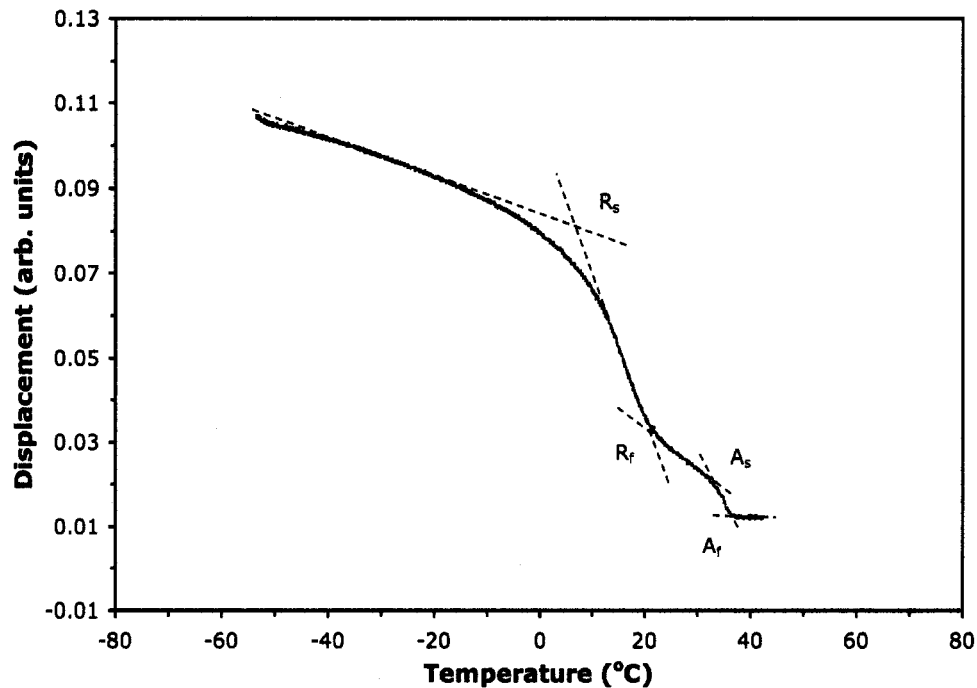
Figure 12. Two-stage transformation.

point where displacement ceased. Also shown in Figure 12 are the R-phase start (R_s) and

R-phase finish (R_f) temperatures, which correspond approximately to the temperatures

where the transformation from martensite to the R-phase starts and finishes.

During the BFR study, three specimens per heat treatment condition were used to

determine the scatter of the A_f data. Wire in the as-drawn condition and after heat

treatment at 300°C were unable to be tested because of excessive spring back upon

release of the mandrel even after cooling to below -100°C. This spring back is attributed

to the high levels of cold work in the wire. For this reason, BFR testing was performed

only on wires heat-treated at 350 ~ 550°C. A summary of the sample conditions used for

the BFR portion of this study is provided in Table 3.

28

Table 3. BFR Sample Conditions.

Specimens per Condition	Cold Work Conditions (%)	Heat Treatment Temperatures (°C)	Heat Treatment Times (min.)	Total number of Specimens
3	30, 50	350, 400, 450, 500, 525, 550	2, 5, 10, 20, 60, 180	216

Tensile testing was performed in accordance with the standard test method for superelastic Nitinol - ASTM F2516-05 [19]. Unlike conventional metals, the testing of superelastic Nitinol utilizes a loading and unloading cycle to outline the stress hysteresis created by the austenite-martensite phase transformation. Each wire specimen was loaded to 6% strain, unloaded to a stress of 5 MPa, and then loaded to failure. Upper plateau (UP) and lower plateau (LP) stresses were determined at strains of 3% and 2.5%, respectively, per ASTM F2516-05, as seen in Figure 13. For specimens of 0.5 ~ 2.5 mm diameter the prescribed strain rate is 0.02 inches per minute per inch of gage length. In this study, a gage length of three inches was used, dictating a strain rate of 0.06 inches per minute. The reason for using a slow strain rate is that the austenite-to-martensite phase transformation is exothermic in the forward direction and endothermic in the reverse, which can result in significant heating and cooling during loading and unloading, respectively. In addition, the mechanical properties of Nitinol are extremely sensitive to changes in temperature. Therefore, a slow strain rate is required to allow thermal conduction between the specimen and its surroundings – thus, minimizing temperature variations in the wire.

29
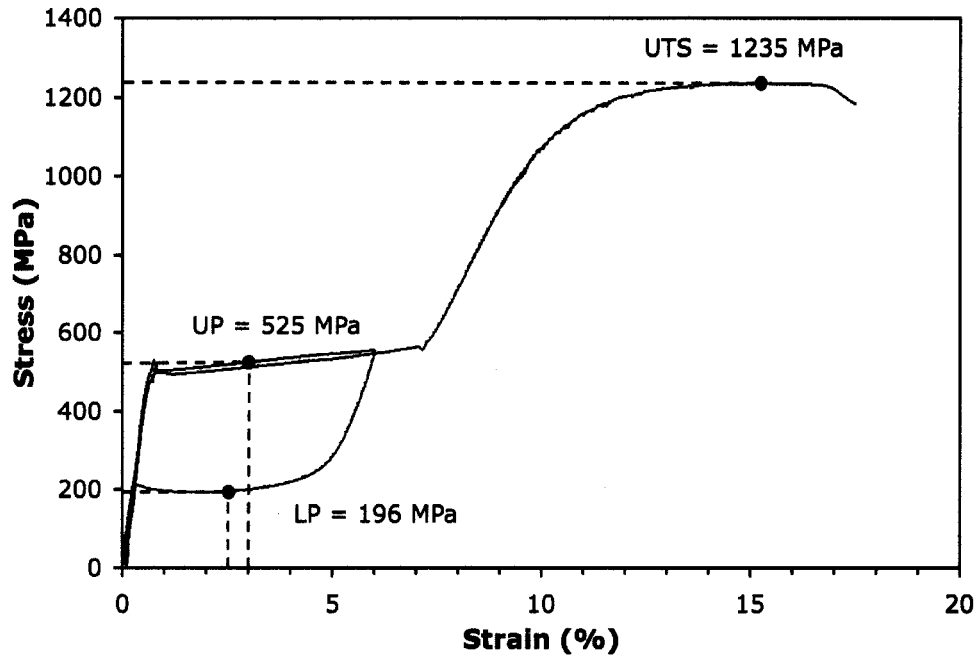
Figure 13. Typical stress-strain response of superelastic Nitinol wire.

One specimen was tested for each heat treatment and cold work condition, except at ten-minute heat treatment times. Two specimens were tested for all ten-minute heat treatments to check the repeatability in the mechanical properties of the wires. The time of ten minutes was chosen because it falls in the middle of the time range and also within the reasonable time limits of a production environment. A summary of the processing conditions of the wires utilized for tensile testing is provided in Table 4.

Two additional heat treatments were performed at 650°C for 60 and 180 minutes. These heat treatments were conducted in an air furnace because the salt pots were limited to temperatures below 600°C. A water quench was performed after the furnace heat treatments. Because these heat treatment times were long, the heat-up times were

30

Table 4. Tensile Sample Conditions.

Specimen per condition	Cold Work Conditions (% $\Delta A_{cs}/A_{cs}$)	Heat Treatment Temperatures (°C)	Heat Treatment Times (min)	Total number of Specimens
1 (2 @ 10min)	30, 50	300, 350, 400, 450, 500, 525, 550, 650[*]	2, 5, 10, 20, 60, 180	102

*650°C heat treatments were performed for 60 and 180 minutes only.

neglected. These heat treatments were added to capture a larger portion of the rapid UTS decrease in the UTS versus heat treatment temperature plots resulting from recrystallization.

CHAPTER FIVE
RESULTS

The changes in the transformational and mechanical properties of the 30% and 50% cold-worked Nitinol wires after heat treatment at 300 ~ 550°C for times of 2 ~ 180 minutes are presented in this chapter. The Ni-rich precipitates that were found in specimens heat-treated at high temperatures for long times are presented in Section 5.1. Changes in transformational properties were characterized with the BFR technique and are presented in Section 5.2. Changes in the mechanical properties were investigated with tensile testing and are described in Section 5.3.

5.1 Scanning Electron Microscopy

The nucleation and growth of Ni-rich precipitates is well documented and commonly utilized in A_f tuning processes [11,13,16]. In this study precipitates were discernable in specimens heat-treated at 525°C and 550°C for times of 60 and 180 minutes. After polishing the specimens, these precipitates were examined using a SEM under backscatter electron emission. The precipitates present in a 50% cold-worked specimen after heat treatment for 180 minutes at 550°C are shown in Figure 14. Smaller precipitates in specimens that were heat-treated for shorter times and at lower temperatures were also detected, but were more difficult to discern and document. Since thermal energy is required to drive the precipitation reaction forward it was expected that larger precipitates could be identified after longer time and higher temperature heat treatments. In general, the precipitates brightness, in contrast to the dark matrix, supports
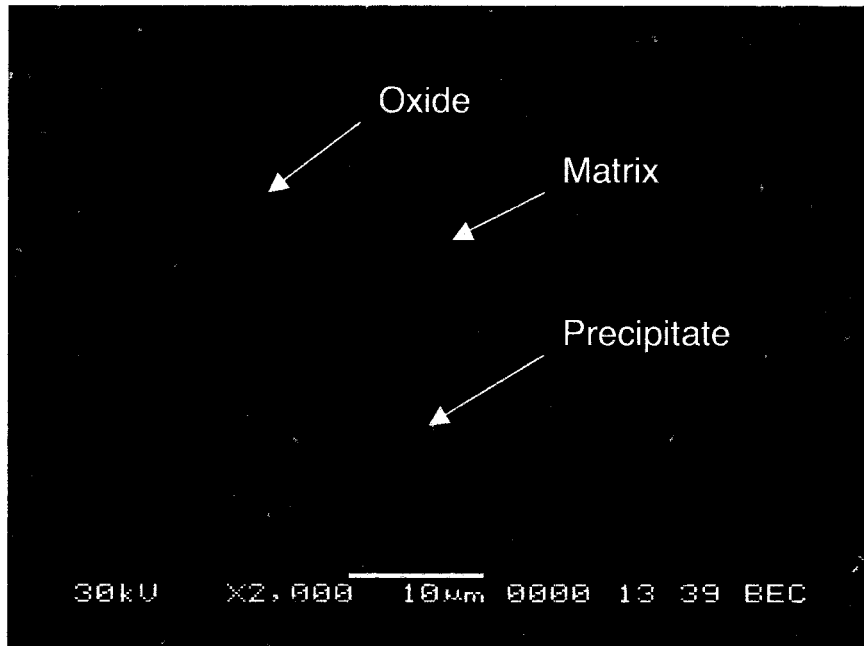
Figure 14. SEM micrograph of 50% cold-worked wire after 180 minutes at 550°C.

the conclusion that they had higher Ni content. This is because Ni, due to its larger size,

has a larger electron scattering cross-section than Ti. Therefore, Ni-rich regions reflect

more electrons and appear lighter than the surrounding matrix. The dark particles shown

in the micrograph are oxide inclusions leftover from the melting process. Compositional

analysis was possible using EDS by focusing the electron spot onto each of the three

phases, *i.e.*, an oxide particle, a precipitate, and the matrix.

The compositional analysis of the three phases obtained from EDS is summarized

in Table 5. These compositional data cannot be used to determine the exact composition

of the precipitates because the spot size was larger than the precipitates, resulting in the

detected signal originating from both the matrix and the targeted precipitate. Further, the

thickness or depth of the phase that is visible at the surface will also play a role in

Table 5. Relative Phase Compositions.

Phase	Ni (wt.%)	Ti (wt. %)	O (wt.%)
Matrix	55.54 ± 0.57*	44.46 ± 0.57	
Precipitate	56.64 ± 0.57	43.36 ± 0.57	
Oxide	36.62 ± 0.82	57.43 ± 1.04	5.96 ± 1.41

*± values are one standard deviation

determining the results of the EDS analysis. In this case the thicknesses were not known, thus reinforcing the argument that the results of the EDS analysis cannot be construed as representing the precise composition of the phases visible at the surface. Qualitatively, however, the EDS data do confirm that the precipitates had a higher Ni content than the surrounding matrix, and that oxygen was present in the dark particles. A complete compilation of the EDS data is included in Appendix B.

5.2 Bend and Free Recovery

This section is divided into four subsections. The changes in the BFR response of the cold-worked Nitinol wires during heat treatment are explained with the use of the BFR curves from wires heat-treated at 350, 450, and 550°C in Section 5.2.1. The presence of the R-phase, in all of the BFR plots, is addressed in Section 5.2.2. The trends in A_f for all heat treatment and cold work conditions are outlined in Section 5.2.3. Two TTT diagrams, one for each level of cold work, illustrating the trends in A_f as a function of time and temperature are presented in Section 5.2.4.

5.2.1 BFR Plots

As mentioned in Section 4.3, BFR tests of both the as-drawn and wires heat treated at 300°C were attempted, but their high levels of stored strain energy prohibited testing. After heat treatment at 350°C and above BFR testing was possible. In this section one representative BFR curve is shown for each of the heat treatment and cold work conditions. The BFR curves have been offset in the displacement axis to avoid overlap. A complete collection of the BFR curves is provided in Appendix A.

The BFR Plots of the 30% and 50% cold-worked wires heat-treated at 350°C are shown in Figures 15 and 16, respectively. In these figures an increase in heat treatment time is seen to translate the austenite-martensite transformation to higher temperatures – a shift to the right. This rightward translation can be quantified as the noted increase in A_f. The A_f increase is attributed to the formation of Ni-rich precipitates depleting Ni from the surrounding matrix and thereby increasing the transformation temperature of the material. Clearly a wide range of A_f temperatures can be obtained from a single starting composition through heat treatment.

The shape of the BFR curves did not significantly change with increased heat treatment time at 350°C. The BFR curves for specimens cold-worked 50% were found to be flatter, *i.e.*, have a lower maximum slope, than those cold-worked 30%. Flatter BFR curves indicate that a higher level of residual cold work remains within the material and impedes the phase transformation. A small transformation strain[††] is an unfavorable result of high residual cold work within the material.

[††] Transformation strain refers to the total strain recovered during the phase transformation.

Figure 15. BFR plots of 30% cold-worked wire after 350°C heat treatments.
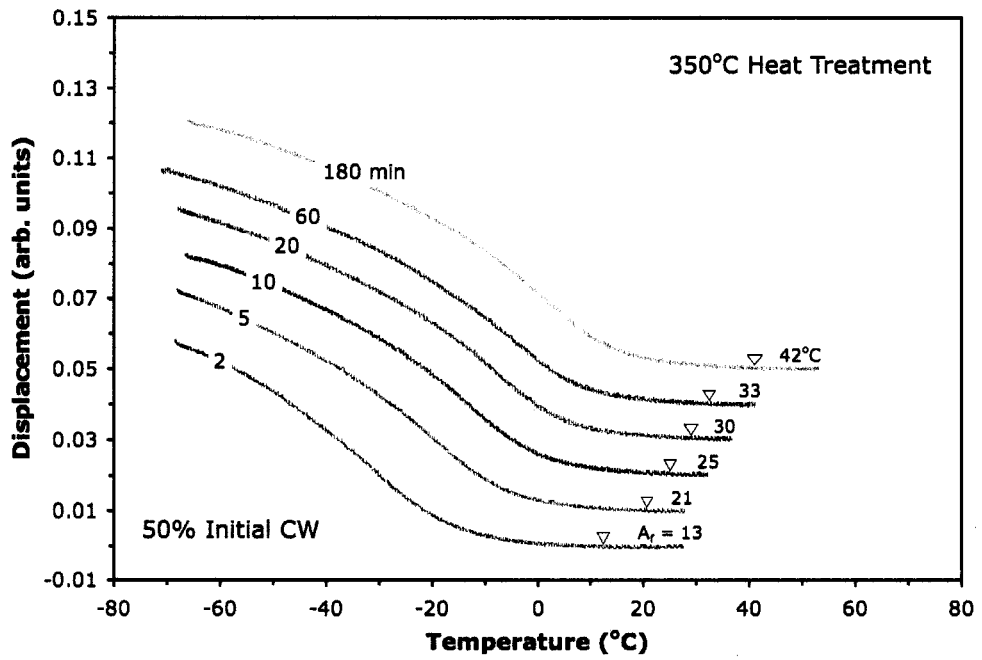
Figure 16. BFR plots of 50% cold-worked wire after 350°C heat treatments.

Relative to the BFR curves from the specimens heat treated at higher temperatures, which are presented later in this section, the onset and end of the austenite-to-martensite transformation are very gradual in the specimens heat-treated at 350°C. In other words, the BFR curves indicated that the transformation is occurring over a wide temperature range and not at one specific temperature. As mentioned in Section 4.3, BFR plots like these, with high curvature, are problematic when determining their A_f. This difficulty leads to more scatter in A_f temperatures obtained from specimens with high levels of residual cold work.

The BFR plots for 30% and 50% cold-worked wires after heat treatment at 450°C are shown in Figures 17 and 18, respectively. An evolution in the shape of the BFR curves can be seen for both levels of cold work during heat treatment at 450°C. The A_f of the 30% cold-worked wire became clearly defined after 60 minutes as the lower curve, or "tail", of the BFR curve was shortened. After heat treatment of the 50% cold-worked wire for 180 minutes, a "step" is noticeable in the BFR curve. This step indicates that a two-stage transformation occurred due to stabilization of the R-phase, as was introduced in Section 4.3. Clear two-stage transformations occurred for the 50% cold-worked specimens heat-treated at 450°C for 60 and 180 minutes.

Prior to the appearance of a clear two-stage transformation, a distinct "flattening" of the BFR tail is seen. These flattened BFR tails also indicate that a two-stage transformation has occurred. Flattening of the BFR tails are seen for heat treatments times of 20 ~ 180 minutes in the 30% cold-worked wire and of 2 ~ 20 minutes in the 50% cold-worked wire. Two-stage transformations were found for the 50% cold-worked wire
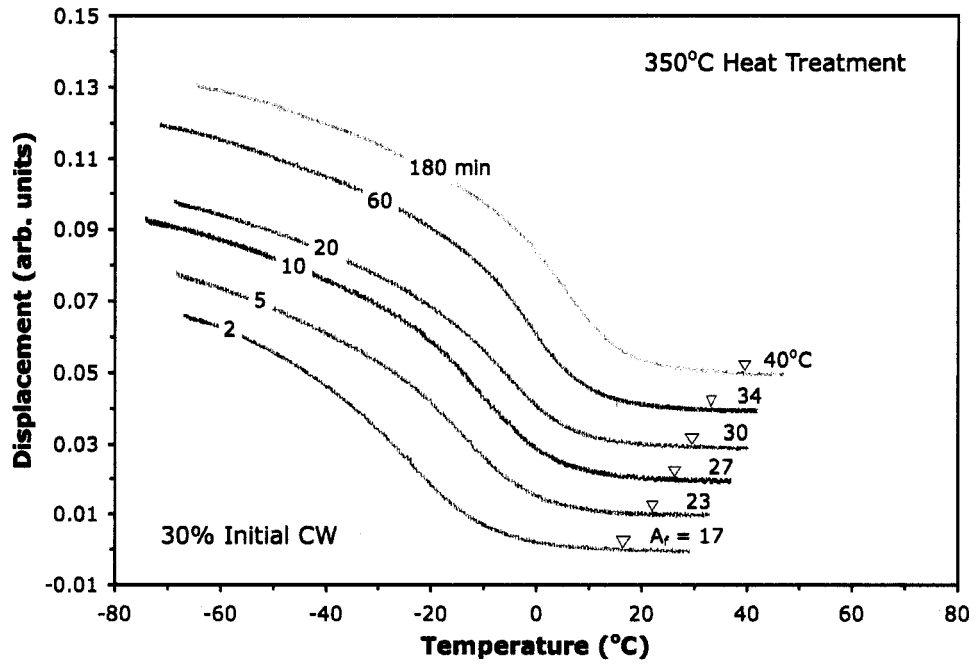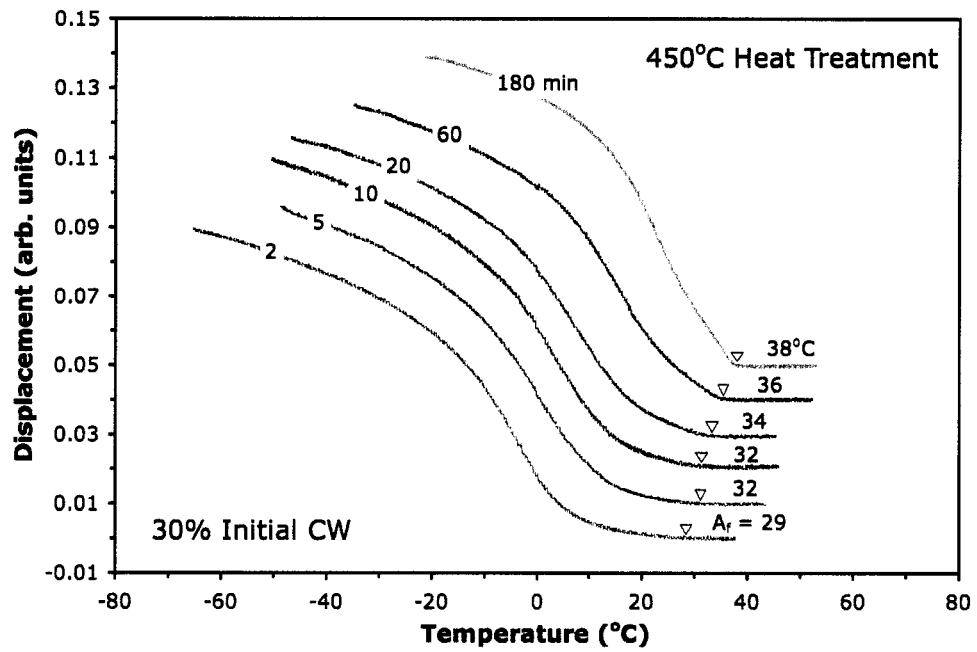
37

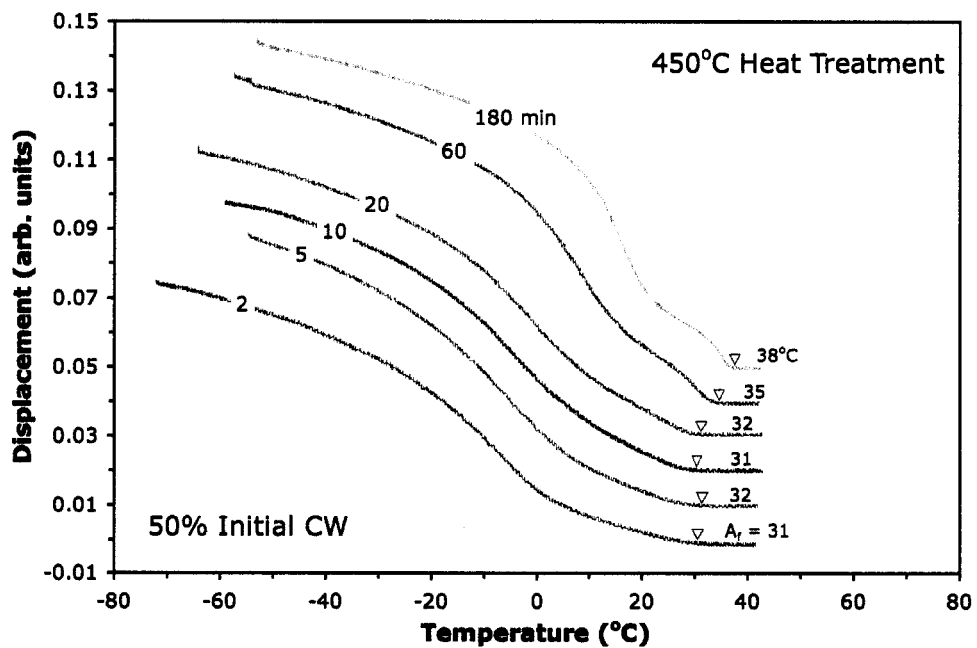Figure 17. BFR plots of 30% cold-worked wire after 450°C heat treatments.

Figure 18. BFR plots of 50% cold-worked wire after 450°C heat treatments.

38

after all 450°C heat treatments and only for 20, 60, and 180 minutes for the 30% cold-worked wire. The greater R-phase presence in the BFR plots of the 50% cold-worked specimens can be directly attributed to the higher level of residual cold work, and therefore stress, in the lattice acting to stabilize the R-phase. A summary of the R-phase presence in all the BFR plots is provided and discussed in section 5.2.2.

As can be seen in Figure 17, the transformation temperatures of the 30% cold-worked specimen heat-treated at 450°C increased with increasing heat treatment time, and corresponding A_f increases occurred. The 50% cold-worked wire, however, showed only a change in the shape of the BFR curves for times of up to 20 minutes, without any significant A_f increase. This is because the BFR tails of the more heavily cold-worked wires were extended at low heat treatment times because of the high level of residual cold work and stabilization of the R-phase. These extended 50% cold-worked BFR tails increased the A_f values beyond those of the corresponding 30% cold-worked specimens. During heat treatment the BFR tails were shortened with increasing time as a result of annealing processes. The shortening of the BFR tails effectively neutralized the expected increase in A_f. The net result was that no significant change in A_f of the 50% cold-worked wire occurred during heat treatments for 2 ~ 20 minutes at 450°C.

The BFR plots for the 30% and 50% cold-worked wire after heat treatments at 550°C can be seen in Figures 19 and 20, respectively. Comparison between the 350°C and 450°C BFR plots and those obtained after heat treatment at 550°C illustrates the dramatic increases in the maximum slope of the BFR curves after higher temperature heat treatments due to the release of stored strain energy during annealing. The BFR plots
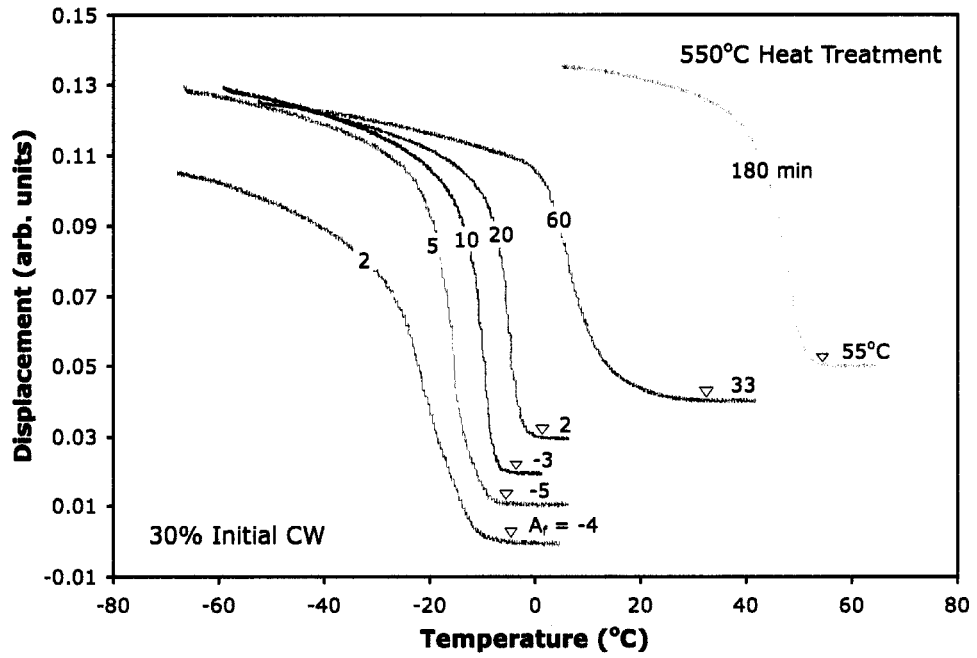
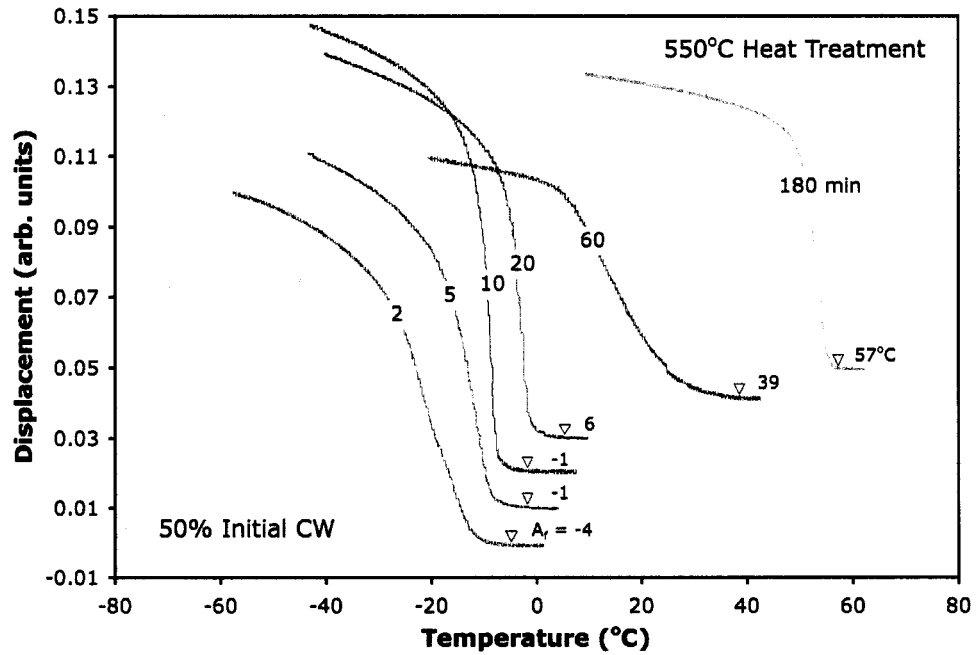Figure 19. BFR plots of 30% cold-worked wire after 550°C heat treatments.

Figure 20. BFR plots of 50% cold-worked wire after 550°C heat treatments.

from both 30% and 50% cold-worked wires show steep recovery occurring after 10 minutes at 550°C. A steep recovery curve means that the transformation occurs over a small temperature range – similar to a step function. This is very desirable for applications such as self-expanding stents because it allows selection of a precise A_f temperature at which expansion is complete.

Heat treatments of 2 ~ 20 minutes at 550°C resulted in lower A_f values than those obtained through heat treatments at 350°C or 450°C, which did not immediately translate to higher A_f temperatures with increased heat treatment time. Following these low A_f temperatures, a rapid increase in A_f occurred during 60 and 180-minute heat treatments at 550°C. The A_f temperatures of 55°C and 57°C were the highest obtained in this study. The initially low A_f temperatures can be attributed to two phenomena: annealing and dissolution of the Ni_4Ti_3 precipitates. As was noted at lower temperatures, annealing acts to increase the slope of the BFR curve and decrease the temperature over which the austenite-martensite transformation takes place – approaching the shape of a step function. At 550°C this change in shape occurred to a large extent after only two minutes, thus shortening the tail of the BFR curve and effectively reducing the A_f in the process. This change in shape is one cause of the relatively low initial A_f temperatures during heat treatment at 550°C.

The second cause for the initially low A_f temperatures during heat treatment at 500°C is the dissolution of the low temperature Ni_4Ti_3 precipitates. This dissolution reaction caused an increase in the Ni content of the surrounding matrix, thereby reducing the A_f of the material. These low A_f temperatures last until the eventual formation of the

41

Ni_3Ti_2 and possibly Ni_3Ti precipitates. It is these later forming, and higher Ni-content, precipitates that were responsible for the rapid A_f increase that occurred after the 60 and 180-minute heat treatments at 550°C.

Heat treatment for 60 minutes at 550°C resulted in distinctly shaped BFR curves for both the 30% and 50% cold-worked specimens. A rapid start and a slow end to the austenite-to-martensite phase transformation distinguish these BFR curves. Similarly shaped BFR curves were seen for 30% and 50% cold-worked specimens heat-treated at 525°C for 180 minutes, *i.e.*, after a lower temperature and longer time heat treatment. This suggests that a specific thermal energy input is required to obtain the structure underlying this BFR response. The exact cause of these uniquely shaped curves was not determined. However, the fact that they occurred at a very specific stage in the heat treatment suggests that a unique microstructure was obtained at these conditions.

5.2.2 R-phase Presence

A synopsis of the R-phase presence in all the collected BFR plots of the 30% and 50% cold-worked wires is contained in Tables 6 and 7, respectively. The absence of the R-phase is indicated in the tables with an "X", a prominent two-stage transformation is indicated with a "P", and the intermediate region where the R-phase began to be apparent with an "I". It can be seen in Table 6 that for the 30% cold-worked wire the R-phase was noted after a total of 13 heat treatment conditions – nine intermediate two-stage transformations and four prominent two-stage transformations. In Table 7 it can be seen that for the 50% cold-worked wire the R-phase was noted after a total of 17 conditions –

Table 6. R-phase Presence in 30% Cold-worked Wire BFR Plots.

30% Initial CW		Heat Treatment Temperature (°C)					
		350	400	450	500	525	550
Heat Treatment Time (min.)	2	x	x	x	I	I	x
	5	x	x	x	P	I	x
	10	x	x	x	P	P	x
	20	x	x	I	P	I	x
	60	x	x	I	I	x	x
	180	x	I	I	x	x	x

Table 7. R-phase Presence in 50% Cold-worked Wire BFR Plots.

50% Initial CW		Heat Treatment Temperature (°C)					
		350	400	450	500	525	550
Heat Treatment Time (min.)	2	x	x	I	I	I	x
	5	x	x	I	P	P	x
	10	x	x	I	P	P	x
	20	x	x	I	P	P	x
	60	x	I	P	P	x	x
	180	x	I	P	x	x	x

eight intermediate and nine prominent. Therefore, the R-phase was present with greater frequency and prominence in the 50% cold-worked wire than the 30% cold-worked wire. This attests to the greater stabilization of the R-phase in a more strained microstructure.

It is interesting to note that two-stage transformations were not observed after heat treatments at 350°C, or after heat treatments at 400°C for times of less than 60 minutes. In addition, there was no R-phase presence noted after heat treatments at 550°C. Therefore, the R-phase was present in the intermediate range of thermal energy input. This suggests that the strain from cold work alone is not enough to stabilize the R-phase. Only when thermal energy is provided to the material, probably facilitating some strain

redistribution, does the R-phase become apparent. This is clearly seen in Figure 16 where heat treatment of the 30% cold-worked wire at 450°C did not initially result in a two-stage transformation. With increasing heat treatment time the R-phase became stabilized and two-stage transformations were apparent after heat treatments of 20 minutes and longer. The disappearance of two-stage transformations after higher temperature heat treatments was due to the release of a significant portion of the stored strain energy within the material. This resulted in the R-phase no longer being stabilized, and one-stages transformations resulted.

5.2.3 A_f Trends

All of the A_f values for the 30% and 50% cold-worked wires are compiled in Figures 21 and 22, respectively. A comparison of Figures 21 and 22 shows that the A_f response during heat treatment was similar for both the 30% and 50% cold-worked wires. The maximum A_f values at short heat treatment times were obtained through heat treatments at the intermediate temperatures of 400°C and 450°C, where the combination of nucleation and growth rates are maximized for the low temperature Ni_4Ti_3 precipitate. Heat treatments at temperatures of 500°C and below, resulted in rapid A_f increases at short times followed by slower increases in A_f at longer times, suggesting the growth of one Ni-rich precipitate – Ni_4Ti_3. The exception to this statement being the 50% cold-worked specimens heat-treated at 450°C, which do not display a rapid increase in A_f at short heat treatment times due to the high levels of residual cold work and the presence of the R-phase. Heat treatment at 525°C resulted in initially low A_f temperatures that
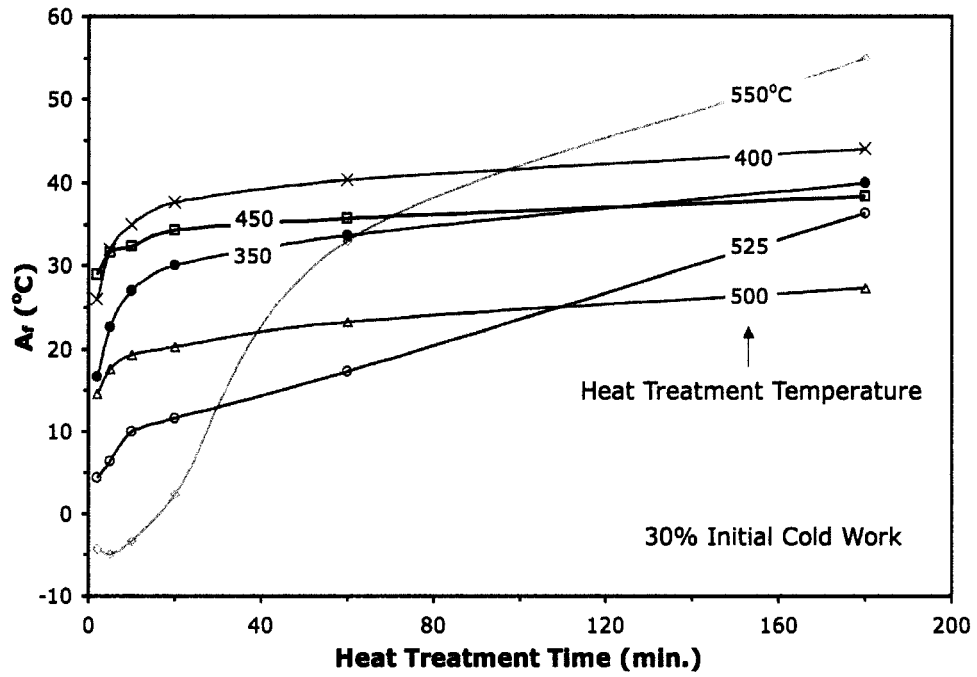
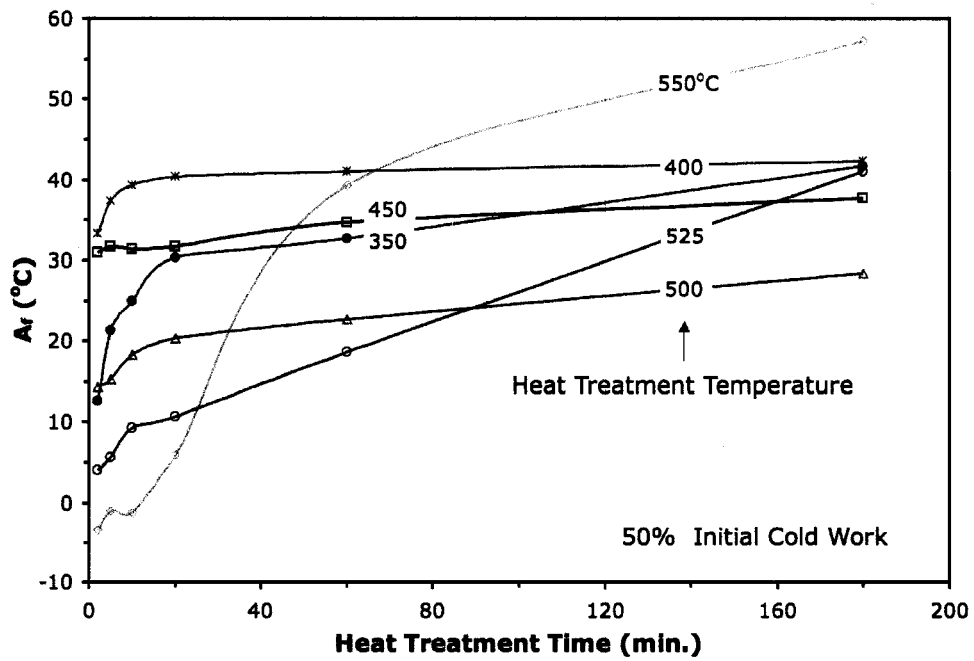Figure 21. A_f trends during heat treatment of the 30% cold-worked wire.

Figure 22. A_f trends during heat treatment of the 50% cold-worked wire.

continued to increase throughout the heat treatment. Heat treatments at 550°C resulted in low A_f temperatures which remained low for times of 2 ~ 10 minutes, followed by a rapid A_f increase during longer time heat treatments. The A_f trends during heat treatment at 525°C and 550°C support the initial dissolution of Ni_4Ti_3 followed by the eventual formation of higher Ni-content precipitates.

It is easy to see that both temperature and time had a significant effect on the A_f temperature of the Nitinol wires. From both the 30% and 50% cold-worked wires a wide range of A_f temperatures were obtained. Therefore, through the careful selection of heat treatment conditions devices with different A_f temperatures, and functions, can be processed from one starting composition.

5.2.4 TTT Diagrams

The two TTT diagrams showing the increase in A_f temperature as a function of heat treatment time and temperature for the 30% and 50% cold-worked wires are shown in Figures 23 and 24, respectively. The two diagrams have similar overall shape. Both diagrams possess a nose at approximately 400 ~ 450°C, indicating the temperature range where the rate of A_f increase was at a maximum. The lines of constant A_f are shifted to the left, *i.e.*, to shorter times, at heat treatment temperatures of 450°C in the TTT diagram of the 50% cold-worked wire. This shift is a direct result of the extended tails of the BFR curves of the more heavily cold-worked wires, as explained in Section 5.2.1. The two TTT diagrams are almost identical in the top portions where heat treatments were at the highest temperatures. Here the annealing processes were highly activated, reducing the
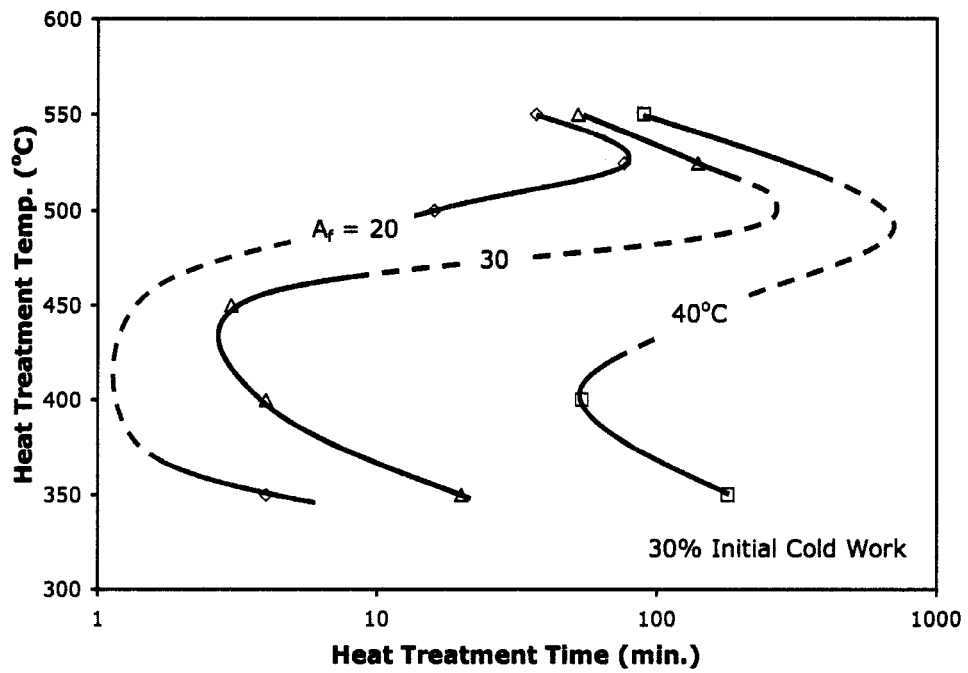
46

Figure 23. General trends in A_f during heat treatment of the 30% cold-worked wire.
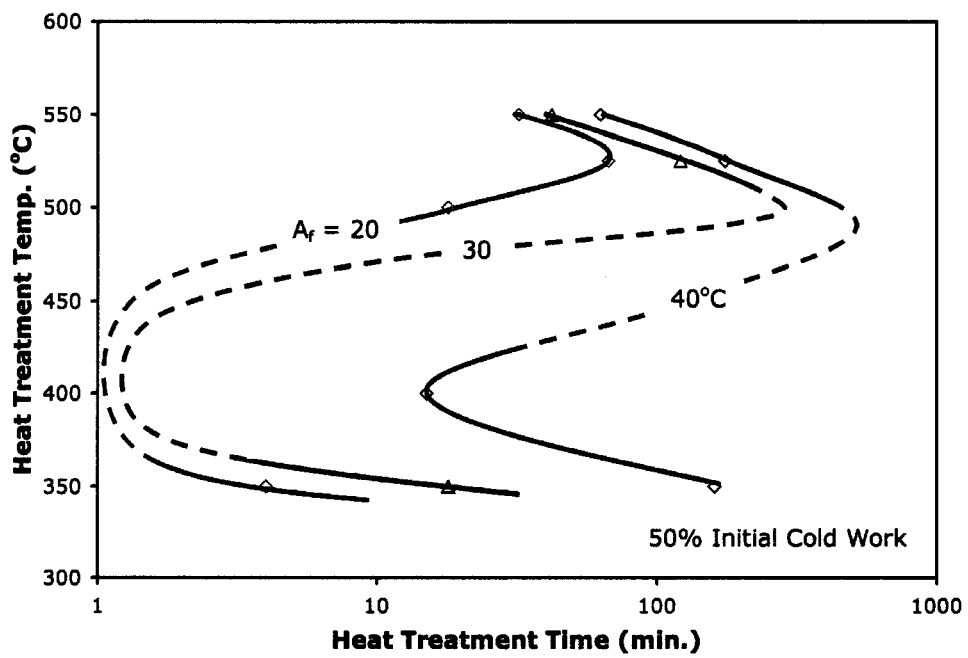

Figure 24. General trends in A_f during heat treatment of the 50% cold-worked wire.

levels of strain energy stored within the wires to comparable levels, regardless of the extent of initial cold work. Although the difference between the lower portions of the two TTT diagrams looks dramatic, it should be noted that these diagrams were constructed with a small number of points and are therefore suitable to illustrate general trends – not as guides for choosing specific heat treatment times and temperatures. For this reason dotted lines are used in the TTT diagrams to indicate regions of the curves where no points were obtained and the lines were drawn based on the expected behavior.

Still, differences between the heat treatment responses of the 30% and 50% cold-worked wires did occur and are significant. Many shape setting and A_f tuning heat treatments are performed in the 450 ~ 500°C range where the A_f was affected by both annealing and precipitation processes. At these temperatures residual cold work was shown to cause extension of the BFR tail, increasing the measured A_f, as well as stabilizing the R-phase. It is therefore important to consider the amount of cold work in the material when selecting a heat treatment time and temperature to obtain a specific A_f.

5.3 Mechanical Properties

This section is divided into four subsections. The tensile responses of the as-drawn 30% and 50% cold-worked wires are described in Section 5.3.1. The changes in the stress-strain diagrams of the wires resulting from heat treatment and residual cold work are presented in Section 5.3.2. The trends in UTS for all heat treatment and cold work conditions are discussed in Section 5.3.3, followed by the trends in UP and LP stresses of the wires in Section 5.3.4.

5.3.1 As-drawn Wires

The stress-strain responses of the as-drawn 30% and 50% cold-worked wires are shown in Figures 25 and 26, respectively. The stored internal strain energy within these specimens was sufficient to inhibit the austenite-to-martensite phase transformation during loading and unloading, resulting in the absence of superelastic behavior. As mentioned in Section 5.2, BFR testing of the as-drawn wires was not possible, even after cooling to -100°C, due to the high level of stored strain energy. Clearly heat treatment was needed to enable the material to change phases.

The UTS of the 30% and 50% cold-worked wires were 1450 MPa and 1900 MPa, respectively. As expected, the as-drawn 50% cold-worked specimen exhibited a higher
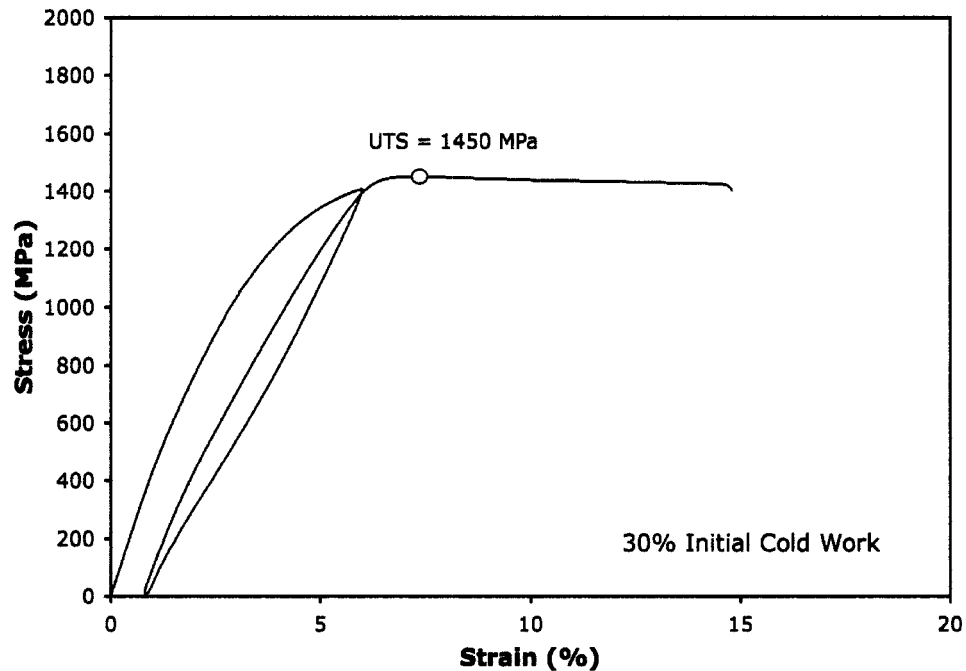

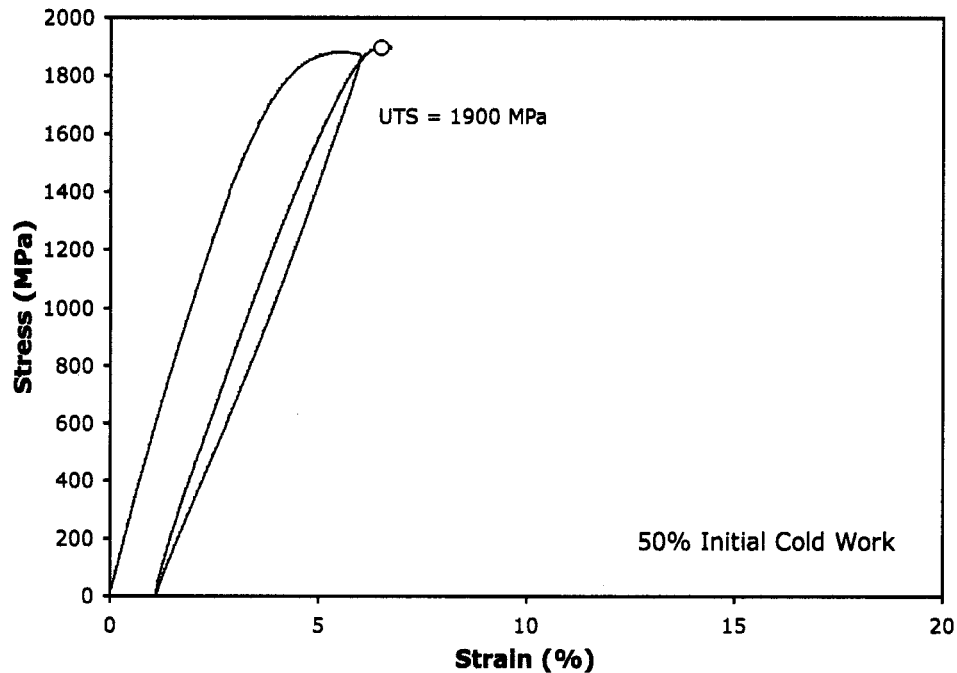Figure 25. The tensile response of the as-drawn 30% cold-worked wire.

Figure 26. The tensile response of the as-drawn 50% cold-worked wire.

UTS and lower ductility than the as-drawn 30% cold-worked specimen. This is the result of the higher strain energy stored within the more heavily cold-worked material.

5.3.2 Stress-strain Diagrams

The tensile response of the 30% and 50% cold-worked wires after heat treatments for 2, 20, and 180 minutes at 300°C can be seen in Figures 27 and 28, respectively. The times of 5, 10, and 60 minutes are not shown to make the figures more readable. It can be seen in Figures 27 and 28 that after heat treatment for two minutes at 300°C, the superelastic flag was regained by both wires, indicating that the low temperature annealing processes had begun. After heat treatment at 300°C the superelastic flags of
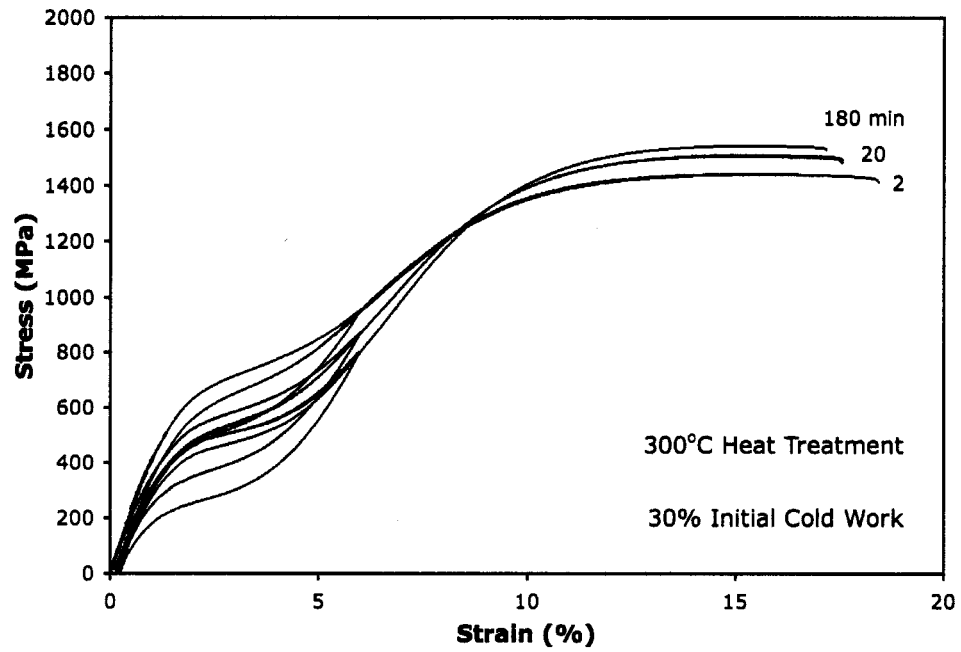
Figure 27. The tensile response of 30% cold-worked wire after 300°C heat treatments.
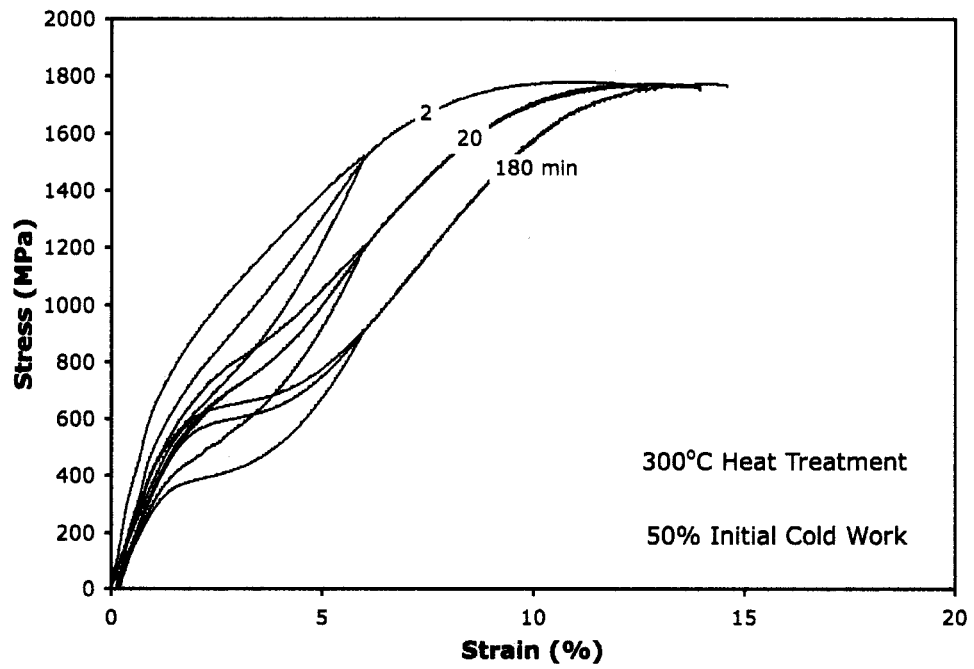

Figure 28. The tensile response of 50% cold-worked wire after 300°C heat treatments.

both the 30% and 50% cold-worked wires were distorted – the upper and lower plateau regions were not plateaus but instead sloped, *i.e.*, the material work hardened during the stress-induced transformation. A greater slope, or higher work hardening rate, was found in the UP and LP regions of the 50% cold-worked specimen. Continued heat treatment at 300°C resulted in decreases in the UP and LP stresses corresponding to the flattening of the superelastic flags. Sloped upper and lower plateaus were also noted for wires heat treated at 350°C. All UP and LP sloping was found to decrease with increased heat treatment temperature and time. The slope of the upper and lower plateaus is attributed to the high levels of residual cold work in the wires.

The slope of the upper and lower plateaus has been explained in more depth by Morgan *et al.* [20]. Morgan attributes this sloping to "elastic strain energy" stored within the material during transformation to martensite, and released during the reverse transformation. This elastic strain energy acts to resist the stress-induced austenite-to-martensite transformation, upon loading, and assist in the reverse transformation, upon unloading. The greater amount of residual strain energy present in the 50% cold-worked wire resulted in a greater amount of stored elastic strain energy during transformation and, therefore, a steeper slope of the superelastic flag. With increased heat treatment time and temperature the residual strains from cold work were released and as a result the slopes of the upper and lower plateaus became horizontal.

Also seen in Figure 27, the UTS of the 30% cold-worked wire increased with increasing heat treatment time. This indicates that the Ni-rich precipitates formed during heat treatment at 300°C act as effective barriers to dislocation motion, thus strengthening

the material. Although recovery processes occurred during the 300°C heat treatment, causing the noted changes in the superelastic flag, the precipitation strengthening effect was sufficient to dominate the trends in UTS in the 30% cold-worked material. The UTS of the 50% cold-worked wire, however, decreased from its as-drawn value after two minutes at 300°C, and remained nearly constant with increasing heat treatment time. This is because the annealing processes were more substantial in the more heavily cold-worked material; therefore, the precipitation strengthening effects were masked.

Heat treatment at 450°C resulted in complete recovery of an undistorted superelastic flag after only two minutes, as shown in Figure 29. During heat treatment at 450°C for 2 ~ 60 minutes the UP and LP stresses decreased as the heat treatment time increased, as can be seen in Figures 29 ~ 31. These decreases are due to the increase in A_f that occurred as a result of precipitation. As the A_f increased the stability of the austenite phase at room temperature was lowered, thereby decreasing the stress required to induce the austenite-to-martensite transformation – the upper plateau stress. Similarly the stress driving the reverse transformation, the lower plateau stress, also decreased.

With increased heat treatment time, the superelastic recovery of the wires was diminished, and between 60 and 180 minutes room temperature superelastic behavior was lost. This can be seen in Figure 32 as the large amount of strain not recovered after unloading. The loss of room-temperature superelasticity was a direct result of the increase in A_f of the wire. Heat treatment at 450°C for 180 minutes increased the A_f of the wire to 38°C, as explained in Section 5.2, and the thermal energy at room temperature was no longer sufficient to drive the transformation back to austenite upon unloading.
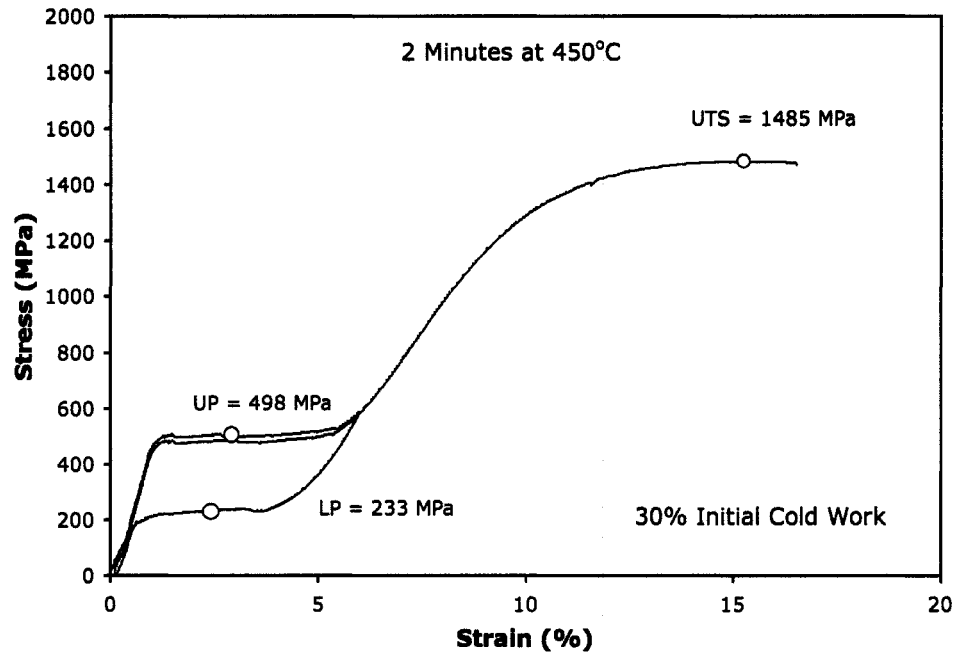
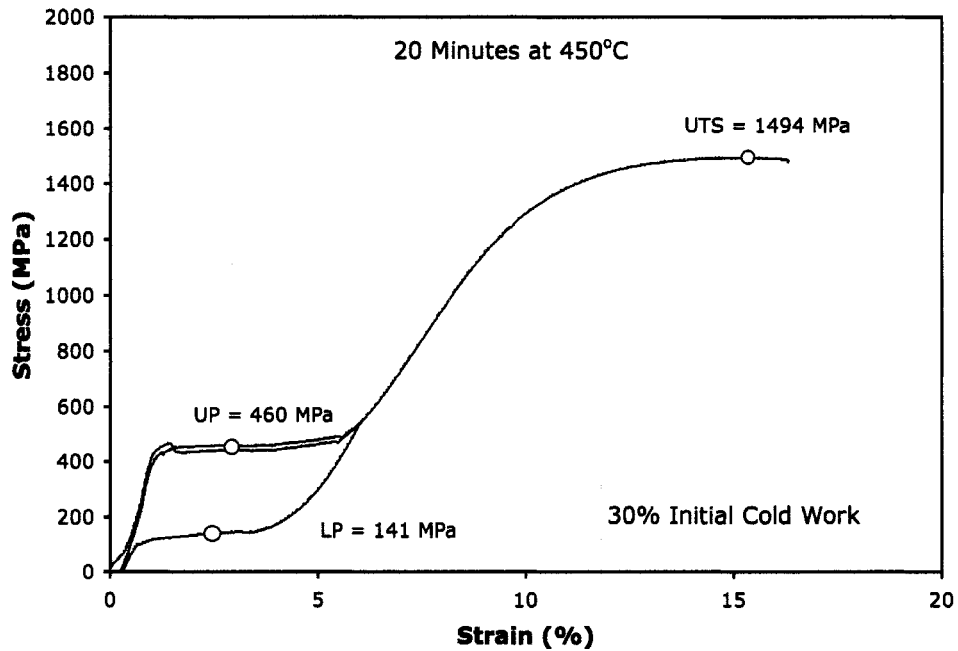Figure 29. Tensile response of the 30% cold-worked wire after 2 minutes at 450°C.

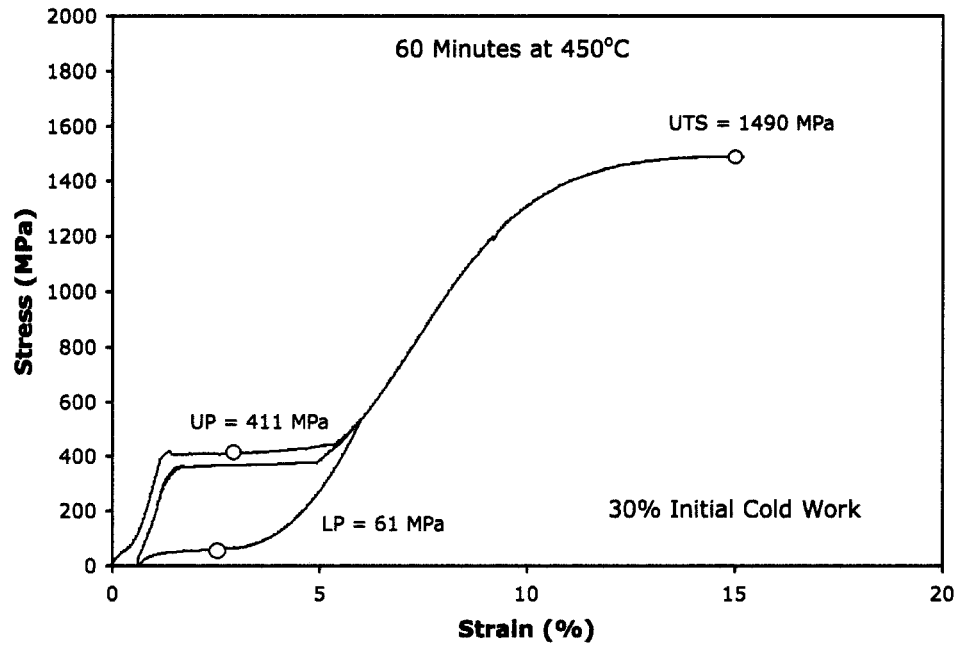Figure 30. Tensile response of the 30% cold-worked wire after 20 minutes at 450°C.

Figure 31. Tensile response of the 30% cold-worked wire after 60 minutes at 450°C.
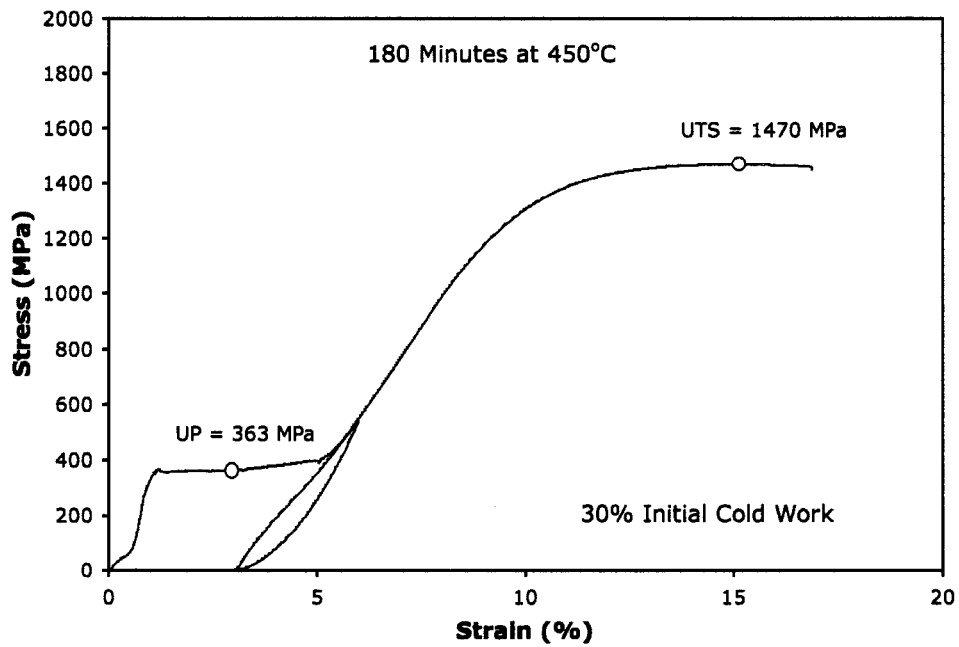

Figure 32. Tensile response of the 30% cold-worked wire after 180 minutes at 450°C.

Heating this wire to above 38°C would have resulted in near complete strain recovery as a result of the shape memory effect.

Stress-induced transformation to the R-phase can be seen as an inflection point, a small step, at the beginning of the linear elastic loading region in Figures 29 ~ 32. Similar to the R-phase presence in the BFR plots, present in Section 5.2, the R-phase became more distinct after longer heat treatment times at 450°C.

The stress-strain response of the 50% cold-worked wire is not shown here because it is similar to that of the 30% cold-worked wire. The only significant difference arises in the UTS trend. The UTS of the 30% cold-worked wire increases during 2 ~ 20-minute heat treatments at 450°C and then decreased with increasing time. The UTS of the 50% cold-worked wire decreased with increasing time for all heat treatments at 450°C. This difference is again attributed to the competition between precipitation strengthening and annealing, with the latter being more predominant in the more heavily cold-worked wire.

5.3.3 Ultimate Tensile Strength Trends

The UTS trends of the 30% and 50% cold-worked specimens for all heat treatment conditions are compiled in Figures 33 and 34, respectively. The UTS of the 30% cold-worked wire is seen to have increased for all heat treatments in the 300 ~ 450°C temperature range.

The UTS increase was largest after 180 minutes at 350°C, where the maximum UTS of the 30% cold-worked wire was obtained – 1567 MPa. This was an increase of 117 MPa from the as-drawn UTS of 1450 MPa. The maximum UTS increase was
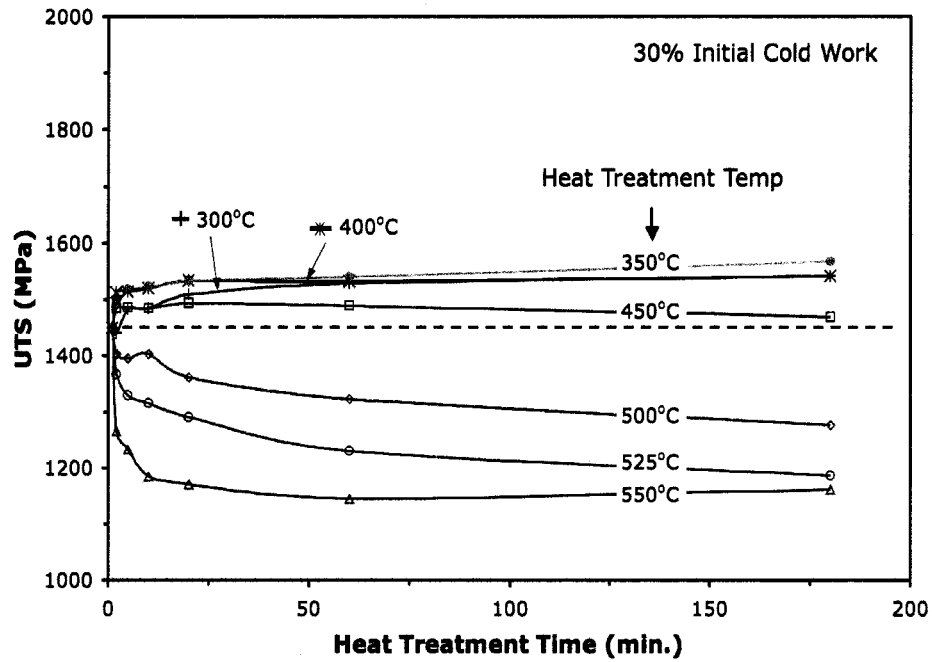
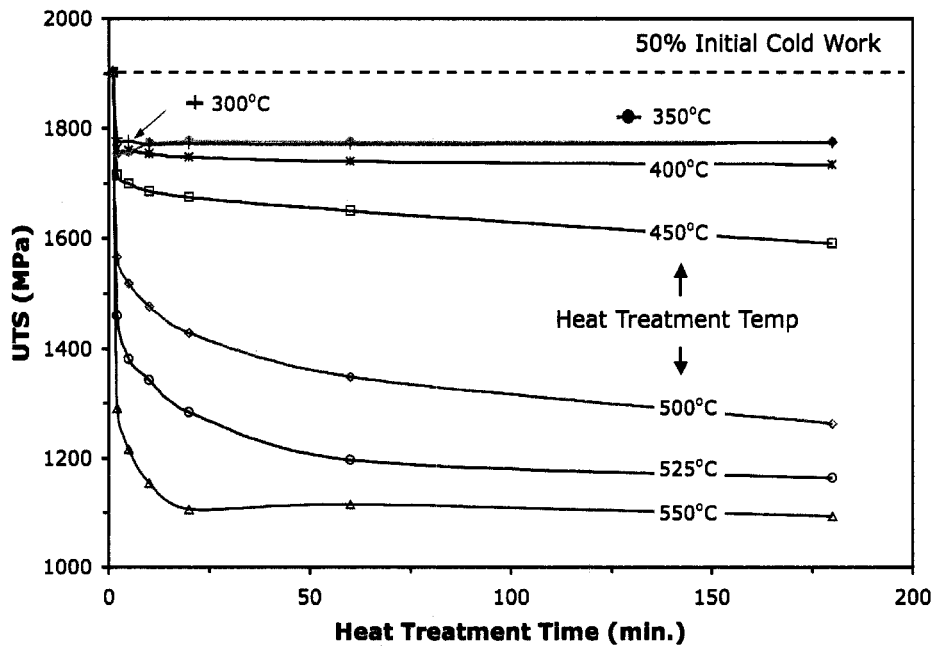Figure 33. Trends in UTS during heat treatment of 30% cold-worked wire.

Figure 34. Trends in UTS during heat treatment of 50% cold-worked wire.

obtained where the combination of strengthening from both precipitation and residual cold work was greatest. Heat treatments of the 30% cold-worked wire at 500°C and above result in UTS decreases as a result of increased annealing.

The UTS of the 50% cold-worked wire decreased for all heat treatment conditions. Higher heat treatment temperatures resulted in larger UTS decreases. At longer heat treatment times, the decreases in UTS diminished. These trends illustrate that higher thermal energy was provided to activate the annealing processes during the higher temperature heat treatments and therefore higher temperature heat treatments allowed the release of more stored strain energy from the cold-worked material. With increased time the material approached a stable microstructure and annealing processes ceased.

In an effort to identify the stages of annealing, plots of UTS as a function of heat treatment temperature were constructed for each heat treatment time. The 10 and 60-minute heat treatment time plots are shown in Figures 35 and 36. The dashed isotherms at 450°C indicate the temperature where a rapid decrease in UTS began. This rapid drop in UTS is attributed to the onset of recrystallization at approximately 450°C [16,21]. This value is a bit lower than half of the absolute melting temperature of Nitinol, 792 K (519°C), which is a rough approximation of the recrystallization temperature. The larger decrease in UTS between 400°C and 450°C in the 50% cold-worked wire than in the 30% cold-worked wire is due to the higher driving force for annealing in the more heavily cold-worked material. The onset of the UTS drop, and therefore recrystallization, also occurred at a slightly lower temperature for the 50% cold-worked wire than for the 30% cold-worked wire for the same reason.
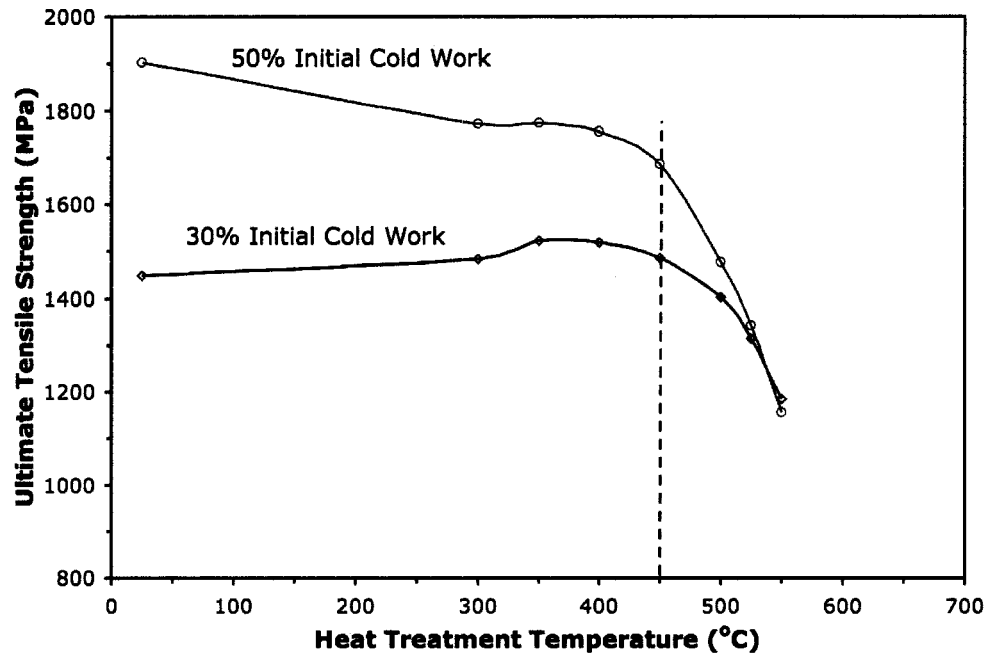
58

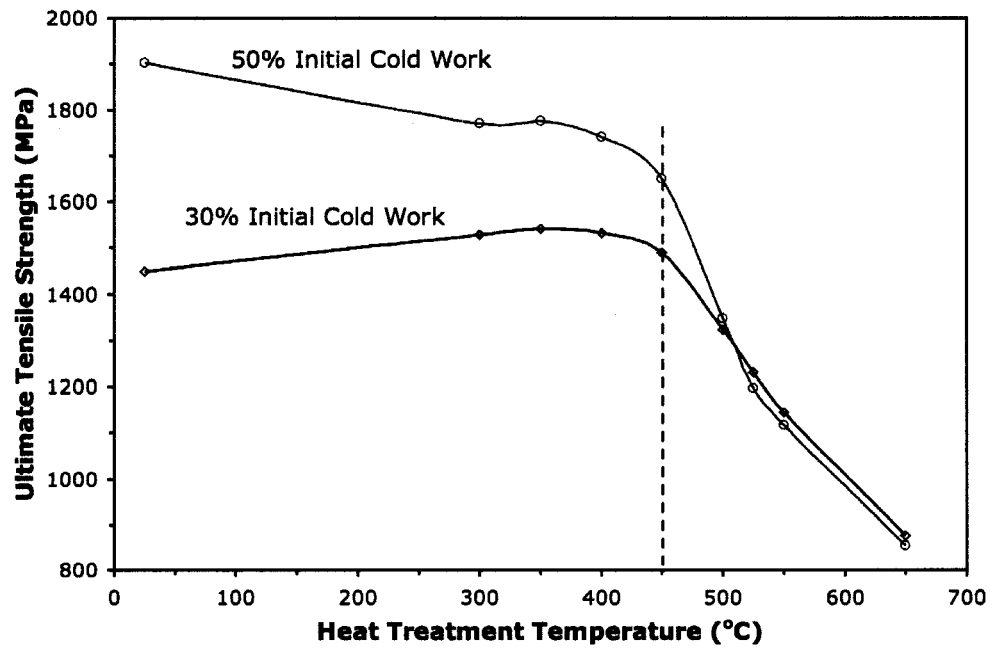Figure 35. UTS trends after 10-minute heat treatments.

Figure 36. UTS trends after 60-minute heat treatments.

Heat treatments at 450°C and below resulted in markedly different UTS values for the 30% and 50% cold-worked wires with the more heavily cold-worked material having higher strength. Heat treatments at these temperatures can be used to tailor A_f while maintaining much of the strengthening resulting from residual cold work. Not surprisingly the highest UTS values were obtained through short heat treatments at low temperatures of the 50% cold-worked wire. Heat treatments at 500°C and above, in contrast, resulted in relatively close UTS values for wires of both 30% and 50% cold work. At these temperatures the annealing processes, including recrystallization, were significantly activated.

Both the 30% and 50% cold-worked wires possessed a slight "bump" in UTS between the temperatures of 350°C and 450°C. These bumps correspond to the increases in UTS as a result of precipitation strengthening. In the 350 ~ 450°C temperature range the precipitation reaction was most effective at strengthening the material. At these temperatures the Ni_4Ti_3 precipitates form within the grains, causing significant internal strains within the material.

The transition between recrystallization and grain growth occurs when all the cold-worked grains are consumed and new strain free grains impinge upon one another. This transition would have been identified by a slowing of the UTS decrease in the UTS – heat treatment temperature diagram. In this study, however, the UTS decrease did not slow, indicating that after 180 minutes at 650°C the end of recrystallization had not yet occurred. Higher temperature heat treatments than those used in this study would have caused complete recrystallization and eventually activated grain growth processes.

5.3.4 Upper Plateau and Lower Plateau Trends

The trends in UP and LP stresses are shown in Figures 37 through 40. The rapid initial decreases in UP and LP stresses during heat treatments at 300°C and 350°C correspond to the evolution of the superelastic flags, seen in Figures 27 and 28, which is attributed to annealing and increasing A_f. A slower and more linear decrease in UP occurred for heat treatment at the intermediate temperatures of 350 ~ 525°C. This trend is attributed mainly to the increase in A_f occurring at these temperatures, as discussed in Section 5.2.3. Heat treatment at 550°C resulted in a rapid decrease in UP stress between the heat treatment times of 20 and 60 minutes. This drop corresponds directly to the rapid A_f increase occurring at these conditions, noted in Section 5.2.3. The spread of the UP and LP stresses was greater for the 50% cold-worked wire, providing access to values different from those obtainable through heat treatment of the 30% cold-worked wire. Absent LP stresses in Figures 39 and 40 indicate heat treatment conditions that resulted in A_f temperatures above room temperature and therefore, the tensile specimen did not exhibit superelastic behavior during testing.

All the trends in tensile properties presented in this section clearly show that both cold work and heat treatment have a dramatic effect on the mechanical and transformational properties of Nitinol. It is also clear that no single property can be altered alone. Therefore, to obtain the ideal balance in properties for a specific application a good understanding of the underlying phenomena must exist. The significant changes in properties, which at first can seem overwhelming and even problematic, actually provide Nitinol its great versatility.
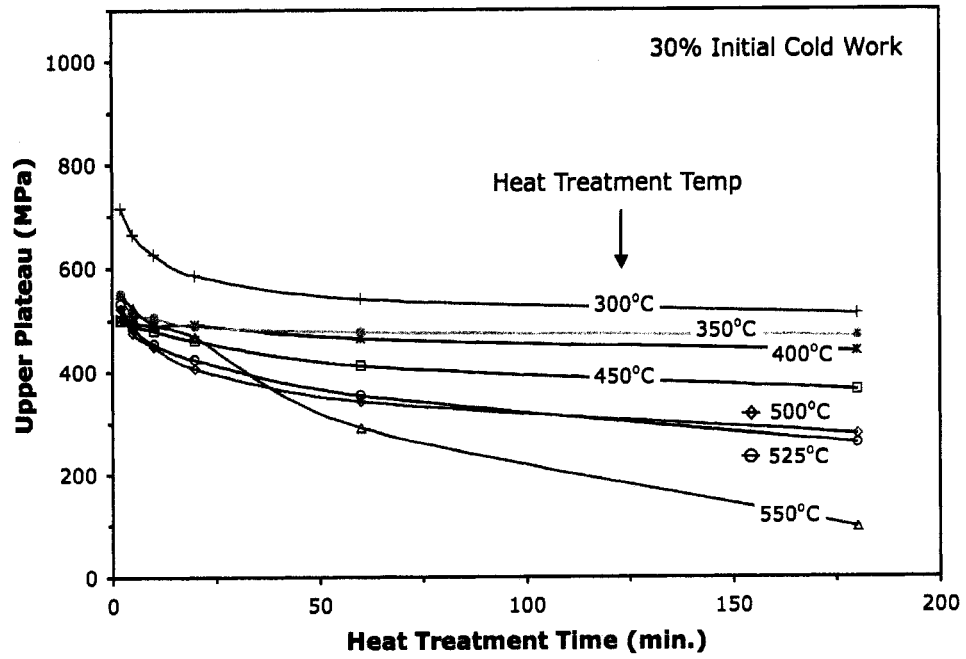
Figure 37. Decreasing UP stress during heat treatment of 30% cold-worked wire.
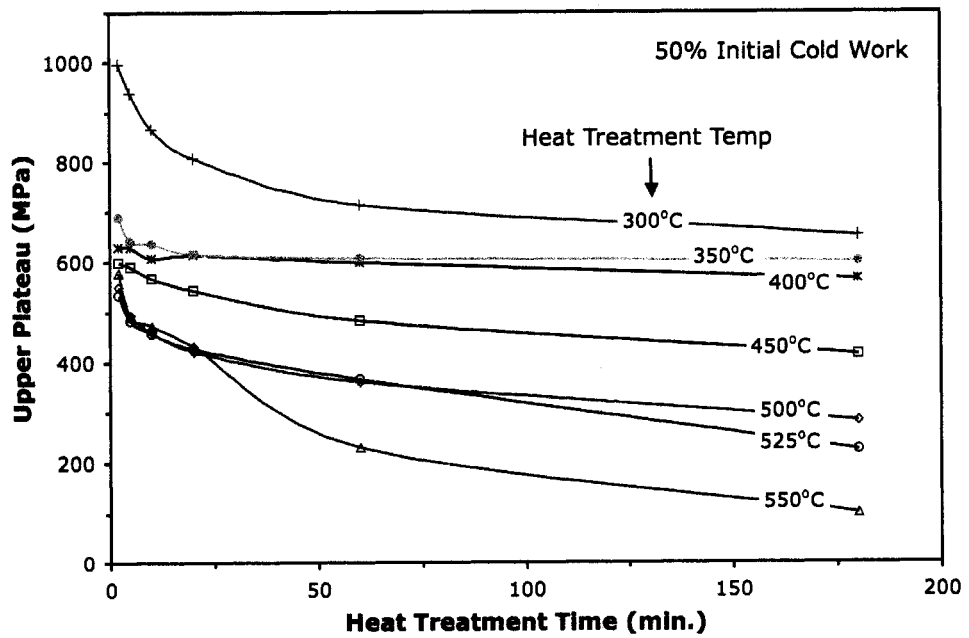

Figure 38. Decreasing UP stress during heat treatment of 50% cold-worked wire.
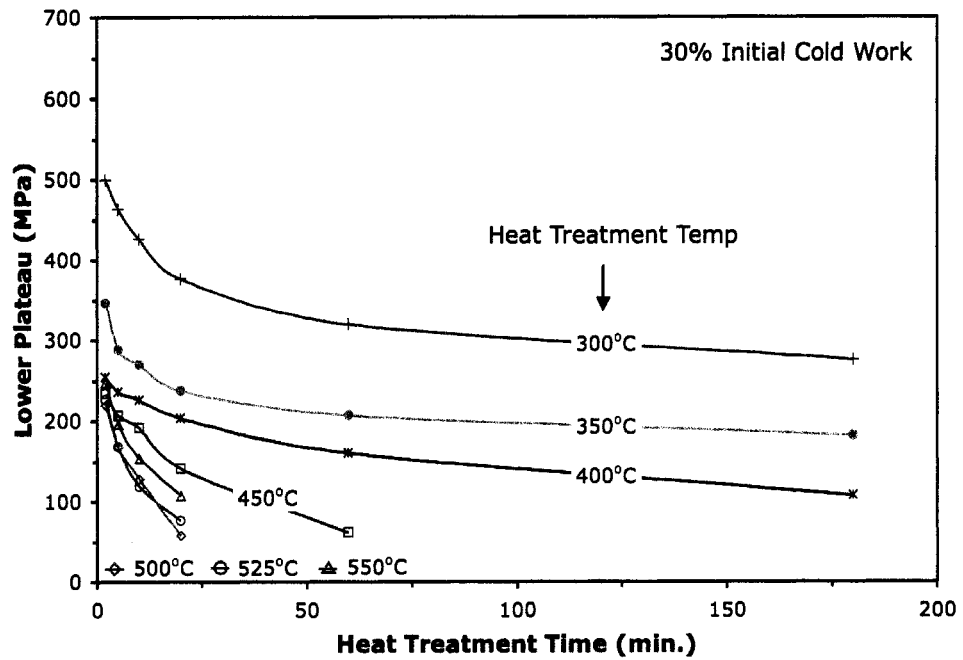
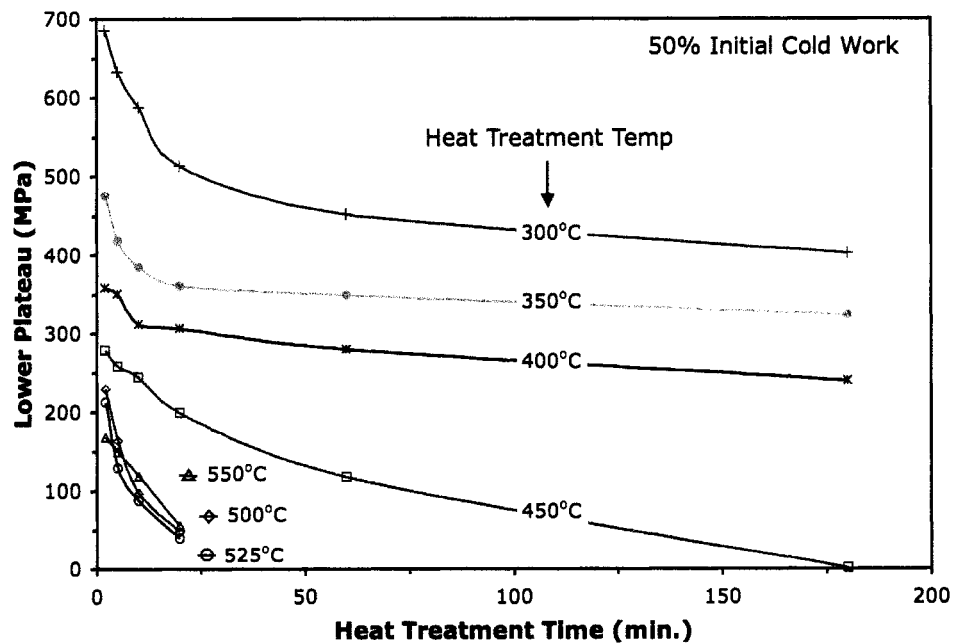Figure 39. Decreasing LP stress during heat treatment of 30% cold-worked wire.

Figure 40. Decreasing LP stress during heat treatment of 50% cold-worked wire.

CHAPTER SIX

DISCUSSION

In this chapter the changes in the transformational and mechanical properties of

the cold-worked Nitinol wires during heat treatment, presented in Chapter Five, are

discussed. This discussion attempts to link the changes in the properties of the wires to

the underlying changes in structure as well as suggest possible benefits of these changes

in product processing. Also, the confidence of the results will be addressed and

comparisons will be made between the results presented in Chapter Five and those

published in relevant journal articles. The discussion is divided into four sections: 6.1

Confidence in the Results, 6.2 Precipitation, 6.3 Annealing, and 6.4 The R-phase.

6.1 Confidence in the Results

As noted in Chapter Four, three specimens per condition were tested in BFR and

only one specimen per condition was tensile tested, the exception being that two

specimens were tensile tested for all 10-minute heat treatments. Larger sample sizes

were not possible within the scope and resources available for this project. From a

statistical standpoint the sample sizes of this research were small. However, the

differences between the two UTS data points of wires heat-treated for 10 minutes ranged

from 0.01 MPa to 30.92 MPa, which represents deviations of 0.0% to 2.2% from the

average values. This can be attributed to the high homogeneity of the wire. Additionally,

the consistency of the trends in the mechanical properties of the wires, when comparing

the different levels of cold work or when comparing different heat treatment temperatures

and times, further supports that the trends resulted from the intentional changes in experimental conditions and not from inadvertent sources of error.

The BFR data were also very consistent among runs and heat treatment conditions. The differences from the average values of the BFR data ranged from 0°C to 2.67°C, which represents deviations of 0.0% to 8.7% from the average values. There tended to be more scatter in the A_f values of wires heat-treated at low temperatures for short times, where high levels of residual cold work extended the BFR tails making it more difficult to determine the A_f. Regardless, the small amount of deviation and consistent trends in A_f allow high confidence in the BFR data.

In addition, the study performed by Pelton *et al.* utilized wire of the same composition and similar heat treatment conditions while monitoring the trends in UTS and A_f [13]. Comparison with the data published by Pelton further supports the trends in the wire properties. A detailed comparison between the data from this investigation and the data from the study performed by Pelton is provided in the following sections.

6.2 Precipitation

The formation of Ni-rich precipitates had two main effects on the properties of the Nitinol wires: strengthening and increasing A_f. Both of these effects are well documented in the literature and supported by theory [10-14].

Precipitation strengthening occurs in Nitinol, as it does in many age hardening alloys, through a specific processing technique. A supersaturated solid solution is created by rapid cooling from a single-phase region, then heat is provided, which activates the

precipitation of a second phase. The formation of this second phase induces stress in the lattice of the primary phase thereby strengthening the material. In this study the increases in strength resulting from precipitation were modest relative to the changes in strength resulting from cold work and annealing. In the case of the 50% cold-worked wire the high internal stresses caused by annealing overshadowed the precipitation strengthening effect and decreases in UTS resulted for all heat treatment conditions. In the case of the 30% cold-worked wire increases in UTS occurred in the $300 \sim 450°C$ range. A maximum strength increase of 117 MPa occurred after 180 minutes at 350°C.

For applications where strength increases are desired heat treatments between 300°C and 450°C can be utilized because precipitation strengthening is most effective in this temperature range. But, strengthening will occur only if the level of cold work of the material is below some critical value between 30% and 50%. If precipitation strengthening does not provide sufficient strength increases then cold working can be used. As can be seen in Figure 35, cold working from 30% to 50% increased the UTS of the Nitinol by 550 MPa. Additionally, a large amount of this UTS increase was retained during heat treatments at 450°C and below.

The ability to modify A_f through the formation of Ni-rich precipitates is very important to the application of Nitinol and is utilized in A_f tuning processes [13]. A range in A_f temperatures of 60°C was achieved in this study by varying the heat treatment conditions. This A_f range allows the production of very different devices from one starting composition. The two TTT diagrams provided in Figures 23 and 24 best illustrate the general trends in A_f. The general shape of the two TTT diagrams agrees

66

well with the TTT diagram constructed by Pelton, shown in Figure 7 [13]. The shape of these TTT diagrams can be well understood through the discussion of nucleation and growth processes presented in Section 2.3. Briefly, at low temperatures growth rates are low, leading to a slow A_f increase, while at high temperatures nucleation rates are low, also leading to a slow increase in A_f. At an intermediate temperature the highest combined nucleation and growth rate results in a maximum rate of formation of Ni_4Ti_3 and therefore a maximum rate of increase in A_f. This is seen as a nose in both of the TTT diagrams of the wires, at approximately 425°C. The nose of the TTT diagrams presented here are consistent with the nose in the TTT diagram constructed by Pelton, which lies at approximately 450°C. Furthermore, Miyazaki *et al.* have reported a maximum precipitation rate of Ni_4Ti_3 at 400°C, which is also consistent with the TTT diagrams of this study and the study by Pelton [13,16].

An understanding of the TTT diagrams presented is essential to the successful processing of Nitinol. The fact that the properties of Nitinol are highly dependent on A_f requires that precise heat treatments be used to set precise A_f temperatures. Although the note is made that the TTT diagrams provided in Figures 23 and 24 should not be expected to provide the exact heat treatment temperatures and times for a given A_f, these diagrams do show that specific A_f values can often be obtained through heat treatment over a range of temperatures. Therefore, when selecting a heat treatment time and temperature, factors such as changes in the recovery behavior, changes in the mechanical properties, and processing time should all be considered. For example a self-expanding stent may require an A_f of 34°C so that it will completely deploy when heated to body temperature.

Therefore, a heat treatment temperature of near 425°C could be used during A_f tuning, so that a rapid A_f increase will shorten the required heat treatment time. An orthodontic archwire, however, may not require such a high A_f but instead benefit from higher strength. In this case, a lower heat treatment temperature, say 350°C, could be used during A_f tuning, so that strength gains, from prior cold working, can be maintained.

Dissolution of Ni_4Ti_3 has been previously reported in the temperature range around 550°C at times less than 20 minutes [13]. This dissolution reaction allows the A_f to be reduced through short heat treatment times at high temperatures. The ability to decrease the A_f of a processed Nitinol component with a short heat treatment at 525°C or 550°C can be very valuable. This is because after high material and processing costs a near complete Nitinol component can be over heat-treated, resulting in a higher than desired A_f. If there were no easy way to decrease the A_f at this point the part would be lost. However, short, high temperature heat treatments can be used to decrease the A_f and thereby save the part.

Although it was thought that a more rapid precipitation rate in the more heavily cold-worked wire might result in a more rapid increase in A_f, this could not be determined. This could be because the dislocation density had no effect on the nucleation rate of the Ni-rich precipitates or because the BFR method was not accurate enough to detect any A_f differences. The increases in A_f that were found in the more heavily cold-worked material were the result of residual cold work causing the BFR curves to be flatter and the R-phase stabilized. No connection to an increase in nucleation rate can be made from these results alone.

68

6.3 Annealing

The high amount of strain energy stored within the as-drawn wires inhibited the ability of the material to transform between the austenite and martensite phases. Not surprisingly, when provide heat these strains were released through the processes of annealing, which had two main effects on the cold-worked Nitinol: softening the material and allowing the phase transformation to proceed more readily.

The decreases in UTS of both wires during heat treatment illustrate a clear reduction in stored internal strain energy. Similar to the 30% cold-worked wire in this research, Pelton also reported decreases in UTS for heat treatments at 500°C and 550°C as a result of annealing. The exact UTS values do not correspond between the two studied because the wire used in the study by Pelton was subjected to a short time straightening anneal at approximately 500°C after drawing, to allow measurement of a starting A_f, while the wires used in this study were not subjected to any initial heat treatment. However, the general trends in the UTS of the wire used in the study by Pelton and the 30% cold-worked wire in this study are otherwise consistent [13]. Understanding that an increased driving force for annealing was present in the more heavily cold-worked specimen, as explained in Section 2.4, makes it easy to transition between the UTS trends of the 30% and 50% cold-worked wires. In short, the annealing processes in the 50% cold-worked material dominated precipitation-strengthening effects, causing decreases in the UTS at all heat treatment conditions. Higher temperature heat treatments further activate annealing – leading to lower stress and lower energy microstructures.

The increase in the slope of the BFR curves and the flattening of the upper and lower plateau regions of the superelastic flags both indicate that the austenite-martensite phase transformation proceeds more readily when increased heat treatment time and temperature reduce the amount of strain energy within the material. After 10 minutes at 550°C, both 30% and 50% cold-worked wires produced steep BFR curves, indicating that the martensite-to-austenite transformation occurred readily as the temperature of the wires were increased.

The residual strains in the 50% cold-worked wire were significant enough to maintain higher UTS values than the as-drawn 30% cold-worked wire after heat treatments at 450°C and below. Also, at these heat treatment temperatures superelastic and shape memory behavior was demonstrated. Therefore, residual cold work is an effective means of strengthening Nitinol while not necessarily prohibiting its unique properties.

6.4 The R-phase

The R-phase was clearly present in many of the BFR plots as well as some of the tensile stress-strain curves of this study. The presence of the R-phase became apparent as heat treatment temperature and time increased until some point after which it was observed to diminish with further thermal energy input. In addition, the R-phase was stabilized to a greater extent in the 50% cold-worked wire than the 30% cold-worked wire. Otsuka [22] has previously reported that the R-phase can be stabilized by three techniques:

(1)   The presence of rearranged dislocations, from cold work followed by heat
treatments at 400 ~ 500°C

(2)   The introduction of fine precipitates, by solution treatment and aging
alloys of 50.8% (at.%) or greater Ni content at 400 ~ 500°C

(3)   The addition of a third alloying element such as Fe and Al

Since both conditions one and two were met in this study, it is not surprising that the R-phase was present in many of the BFR plots recorded. A comparison of the data in Tables 6 and 7 shows that the greater amount of residual cold work present in the 50% cold-worked wire resulted in an increase in both the prominence and frequency of the R-phase presence.

Stabilization of the R-phase through cold work followed by heat treatment, as well as, through the precipitation of Ni_4Ti_3 has been explained in greater detail by the work of Ren *et al.* [23]. Ren explains that both a rearranged dislocation network and the fine dispersion of Ni_4Ti_3 precipitates introduce stress to the lattice, which suppresses the austenite-to-martensite transformation, exposing the intermediate R-phase. The requirement that the dislocation network is rearranged explains why the R-phase was not noted in the as-drawn wires or after low temperature heat treatments, which apparently did not provide sufficient thermal energy to allow the required amount of rearrangement.

The R-phase can cause a great deal of confusion in the processing of Nitinol. Although many engineers would like to avoid the R-phase altogether, high residual cold work is favorable in many applications where strength is of key importance. Therefore,

the R-phase must be accepted and understood. The results of this research do not attempt to provide a complete understanding of the R-phase, but these results do provide an outline of where the R-phase can be expected, in a useful range of heat treatment and cold work conditions.

CHAPTER SEVEN
CONCLUSIONS

The shape memory and superelastic properties of Nitinol, coupled with its biocompatibility, make it suitable for use in applications where conventional engineering alloys would never be considered. These properties inspire the design of novel devices, which exploit the unique capabilities of the material. As more design engineers become award of Nitinol, a change in paradigm is occurring. The successful application of Nitinol requires conceptualizing metals in a new way, thus enabling functionality never before imagined.

Each individual application of Nitinol will place specific demands on the properties of the material. To obtain the optimum balance of the desired properties for a given application, a precise processing technique must be developed, and fine-tuned over time. For this reason, the processing of Nitinol requires an in-depth understanding of the trends in properties during heat treatment at a wide range of temperatures and times, as outlined in this study. In addition the effects of prior processing steps can alter the materials response to heat treatment, and therefore must be considered.

It was found during this investigation that cold work and heat treatment are effective means to modify both the transformational and mechanical properties of Nitinol. The level of cold work was shown to alter the response of Nitinol to heat treatment. The trends in the properties of cold-worked Nitinol during heat treatment can be summarized as follows:

- A maximum rate of A_f increase is obtained at intermediate heat treatment temperatures, namely, at approximately 425°C

- Increased heat treatment time tends to increase A_f

- Higher levels of residual cold work result in higher A_f values, shifting the TTT diagram to the left

- Increased heat treatment time and temperature tend to decrease UTS, UP, and LP stresses although some precipitation strengthening can be achieved through heat treatments in the range of 350 ~ 450°C.

What is also evident from this study is that the mechanical and transformational properties cannot be altered independently. The thermal energy provided during heat treatment will activate both annealing and precipitation processes. Therefore, ultimately it is an understanding of the underlying phenomena – precipitation, recovery, and recrystallization – that will facilitate precise processing of Nitinol.

CHAPTER EIGHT
RECOMMENDATIONS FOR FUTURE WORK

A universal definition of A_f and a consistent method of determination would greatly reduce the current ambiguity. The definition of A_f is currently a point of contention and can create confusion between vendors and customers. The application of Nitinol, however, requires a consistent definition. As described in Section 4.3.1, the ASTM BFR method suggests using the intersection of two tangent lines when determining the A_f. In the case of a one-stage transformation one tangent line is fit to the maximum slope of the BFR curve during recovery and another to the flat portion of the BFR curve where recovery is complete. In the case of a two-stage transformation the first tangent line is fit to the maximum slope of the second step in the BFR plot. This technique is commonly employed when determining the A_f. However, as seen in this study, there are times when the R-phase is present but it does not create a clear two-stage transformation. These cases are not addressed in the ASTM standard. A difference in A_f of 10°C is shown in Figure 41, resulting from two different fits of the same BFR curve. A consistent method for defining A_f, one that reflects the metallurgical process underlying the phase transformation, should be agreed upon by industry and researchers, to eliminate this confusion.

The end point of recrystallization, the beginning of grain growth, was not reached in this study. A study outlining the complete UTS versus temperature trend would provide a more complete understanding of where the recrystallization processes end and grain growth begins. Based on current industry processes this temperature is expected to
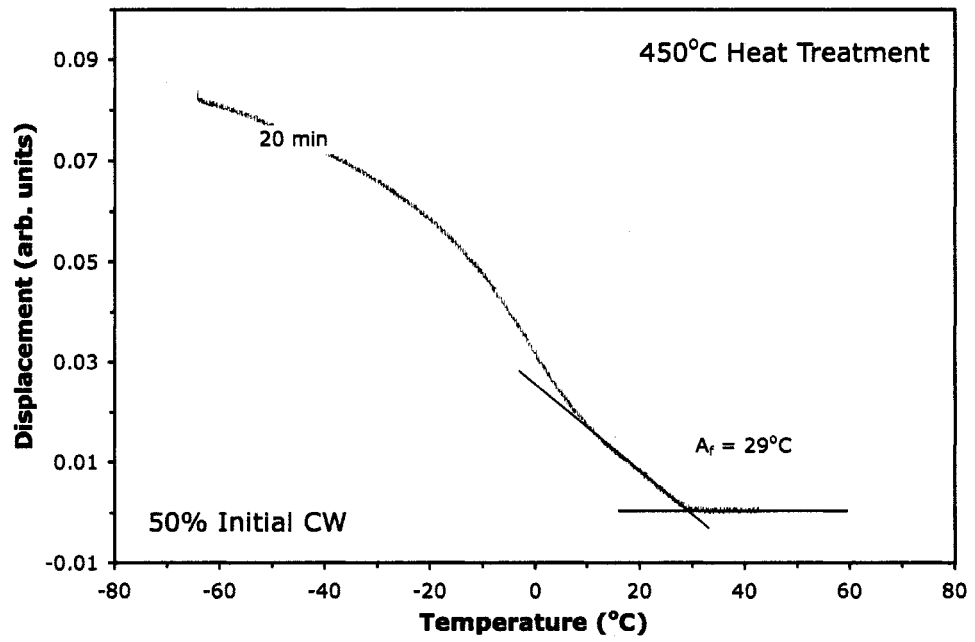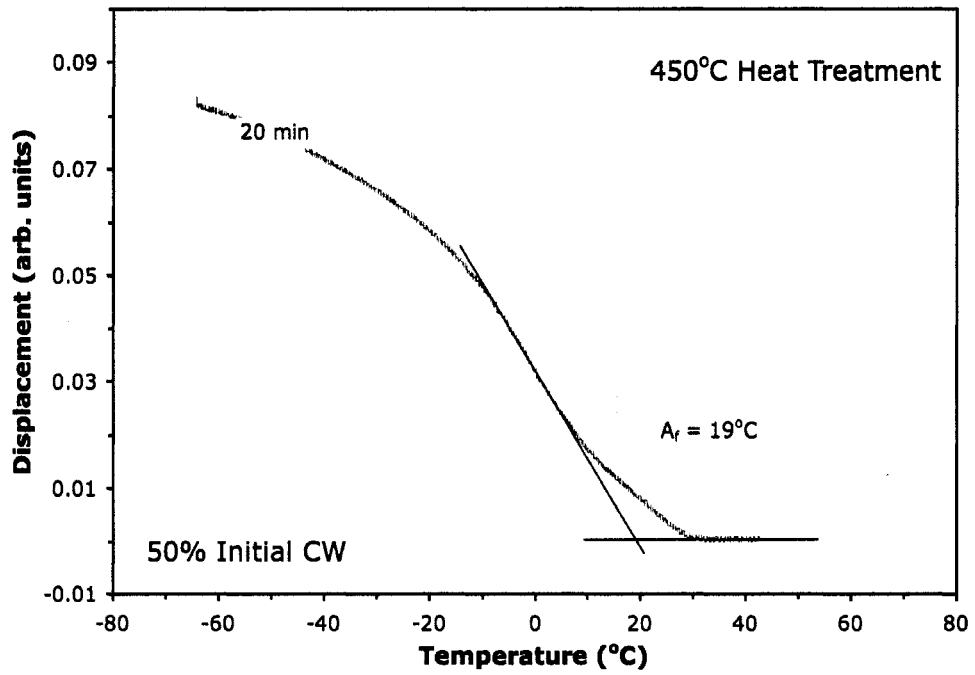
Figure 41. Two fitting methods for the same BFR curve.

be somewhere around 850°C. Heat treatments below 300°C would also be useful in determining the onset of low temperature recovery processes. Such a study would also benefit from the use of transition electron microscopy, which would allow observation of such microstructural changes as rearrangement of the dislocation network, precipitation, and recrystallization.

This study was conducted utilizing the BFR method. A similar study could be conducted utilizing a differential scanning calorimeter (DSC). Using a DSC would involve monitoring the heat flow as wire specimens are heated and cooled through their phase transformations. The transformations are represented in a heat flow diagram as peaks and troughs where heat is absorbed or released by the specimen. This would allow determination of the enthalpy of the transformations and may give insight into the R-phase presence.

Finally, the previous study by Pelton *et al.* [13] that investigated the effects of processing on the properties of Nitinol, compliments the tensile and A_f data with an investigation into the fatigue behavior. The study performed here would also benefit from such an investigation to help correlate the trends in mechanical and transformational properties with the corresponding changes in fatigue properties. The trends in fatigue life must be outlined and understood in order to apply Nitinol in cyclic loading environments, for example, in stents and endodontic files.

REFERENCES

1. G.B. Kauffman and I. Mayo, *"The Story of Nitinol: The Serendipitous Discovery of the Memory Metal and Its Application,"* The Chemical Educator, **2**, (1997).

2. A.R. Pelton, D. Stockel and T.W. Duerig, *"Medical Uses of Nitinol,"* Mater. Sci. Forum, **327**, pp. 63-70 (2000).

3. H. Walia, W.A. Brantley and H. Gerstein, *"An initial investigation of the bending and torsional properties of Nitinol root canal files,"* J. Endodontics, **4**, 346-351 (1988).

4. J.H. Newman, Newman John H. DDS, *private communication (march 2005).*

5. D.E. Hodgson, M.H. Wu and R.J. Biermann, *"Shape Memory Alloys,"* ASM Handbook, **A2**, pp. 897-902 (2000).

6. C.M. Wayman, *"Shape Memory Alloys,"* MRS Bulletin, **18**, pp. 49-56 (1993).

7. T.W. Durig and R Zadno, *"An Engineer's Perspective of Psuedoelasticity,"* in Engineering Aspects of Shape Memory Alloys, pp. 369-393 (1990).

8. K.N. Melton, *"Ni-Ti Based Shape Memory Alloys,"* in Engineering Aspects of Shape Memory Alloys, pp. 21-35 (1990).

9. F.E. Wang, W.J. Buehler and S.J. Pickart, *"Crystal Structure and a Unique "Martensitic" Transition of TiNi,"* J. Appl. Phy., **36**, pp. 3232-3239 (1965).

10. S.M. Russell, *"Nitinol Melting and Fabrication,"* SMST-2000 Conference Proceedings, pp. 1-10 (2001).

11. M. Nishida, C.M. Wayman, T. Honma, *"Precipitation Processes in Near-Equiatomic TiNi Shape Memory Alloys,"* Met. Trans. A, **17A**, pp. 1505-1515 (1986).

12. T. Saburi, *"Ti-Ni Shape Memory Alloys,"* in Shape Memory Materials, edited by K. Otsuka and C.M. Wayman, (Cambridge University Press, Cambridge, United Kingdom, 1998), pp. 49-96.

13. A.R. Pelton, J. DiCello and S. Miyazaki, *"Optimization of Processing and Properties of Medical-Grade Nitinol Wire,"* SMST-2000 Conference Proceedings, pp. 361-374 (2001).

14. R.E. Reed-Hill and R. Abbaschian, Physical Metallurgy Principles, 3rd ed. (PWS-KENT Publishing Company, Boston, USA, 1992), pp. 227-245.

15. H.I. Aaronson, J.K. Lee and K.C. Russell, *"Diffusional Nucleation and Growth,"* in Precipitation Processes in Solids, edited by K.C. Russell and H.I. Aaronson (Metallurgical Soc. Of AIME Conf. Proc., Niagara Falls, NY, 1979), pp. 31-41.

16. S. Miyazaki, *"Thermal and Stress Cycling Effects and Fatigue Properties of Ni-Ti Alloys,"* in Engineering Aspects of Shape Memory Alloys, pp. 394-413 (1990).

17. Ingot Qualification, Nitinol Devices and Components internal document, based on Wah Chang certification (2002).

18. ASTM F 2082, *"Standard Test Method for Determination of Transfomation Temperature of Nickel-Titanium Shape Memory Alloys by Bend Free Recovery,"* ASTM International.

19. ASTM F 2516, *"Standard Test Method for Tension Testing of Nickel-Titanium Superelastic Materials,"* ASTM International.

20. N. Morgan, G. Xiao-Yan, W. Andreas, A. Pelton, *"Observations on Cyclic Transformation Behavior of Nitinol,"* To be published (2005).

21. C.R. Barrett, W.D Nix and A.S. Tetelman, The Principles of Engineering Materials, (PRENTICE-HALL Publishing Company, New Jersey, USA, 1973), pp. 293-302.

22. K. Otsuka, *"Introduction to the R-Phase Transition,"* in Engineering Aspects of Shape Memory Alloys, pp. 36-45 (1990).

23. X. Ren, N. Miura, J. Zhang, K. Otsuka, K. Tanaka, M. Koiwa, T. Suzuki, Y. Chumlykov, M. Asai, *"A Comparative Study of Elastic Constants of Ti-Ni-based Alloys Prior to Martensitic Transfomation,"* Mater. Sci. Eng. A, **312**, pp. 196-206 (2000).
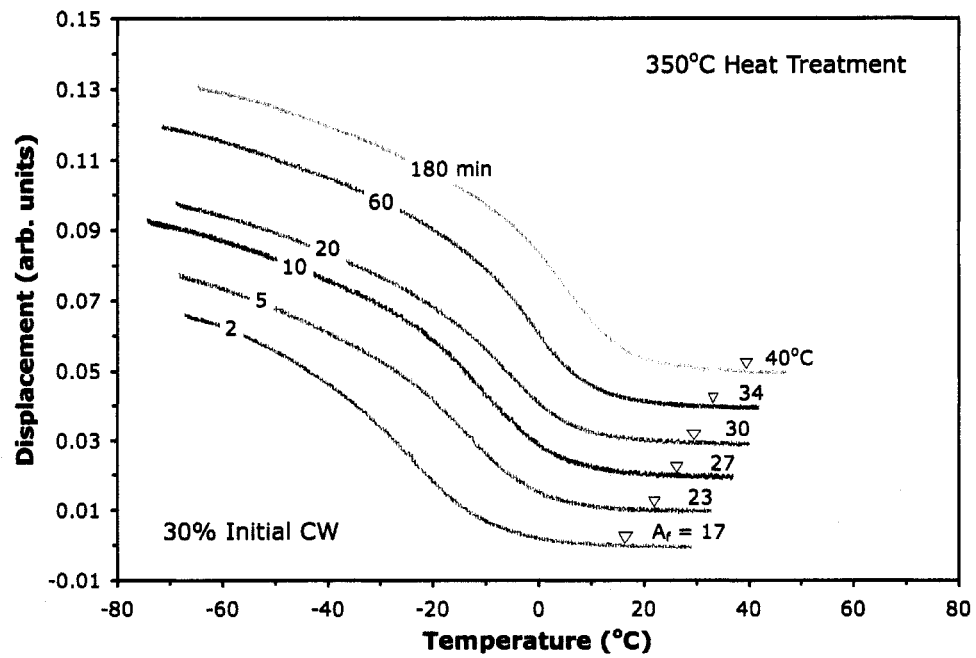
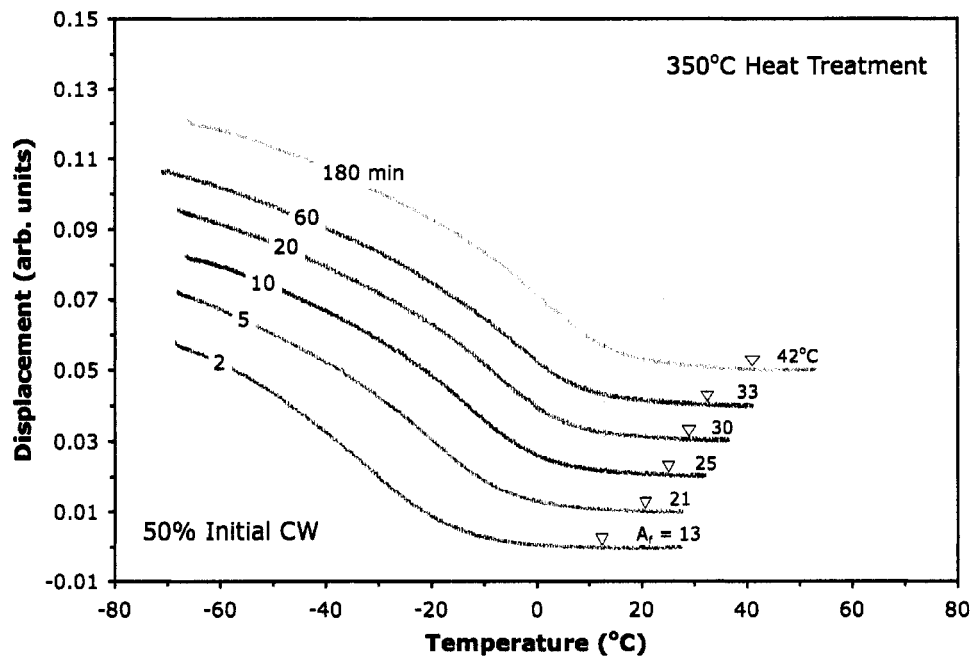Figure A-1. BFR plots of 30% cold-worked wire after 350°C heat treatments.

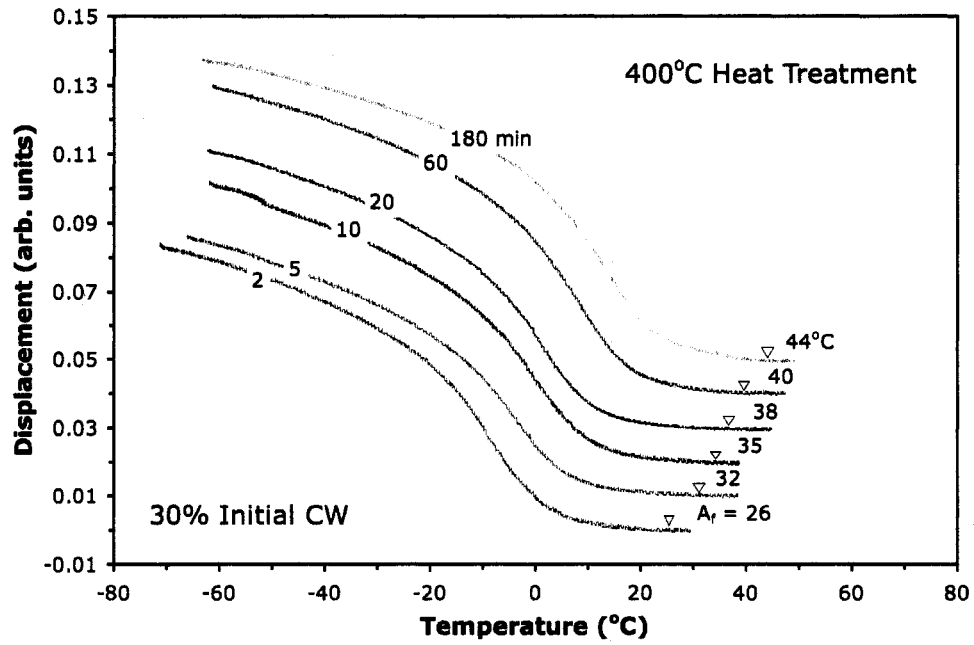Figure A-2. BFR plots of 50% cold-worked wire after 350°C heat treatments.

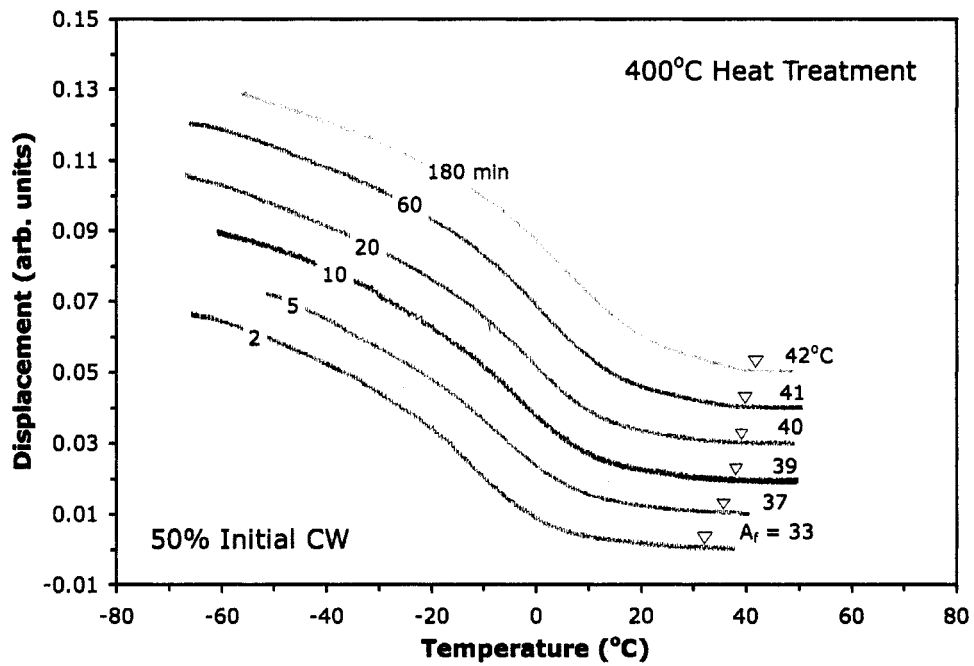Figure A-3. BFR plots of 30% cold-worked wire after 400°C heat treatments.

Figure A-4. BFR plots of 30% cold-worked wire after 400°C heat treatments.
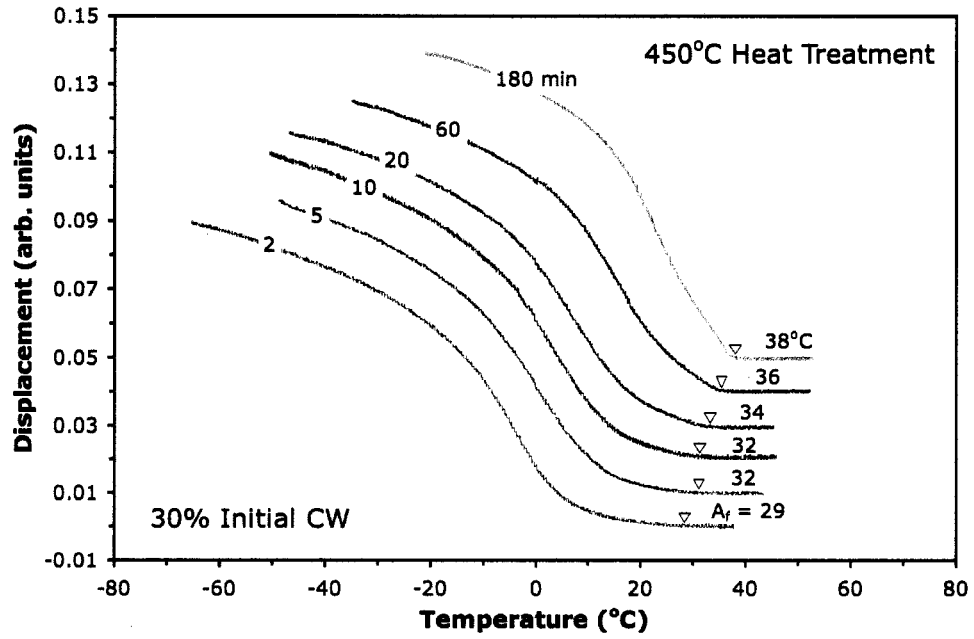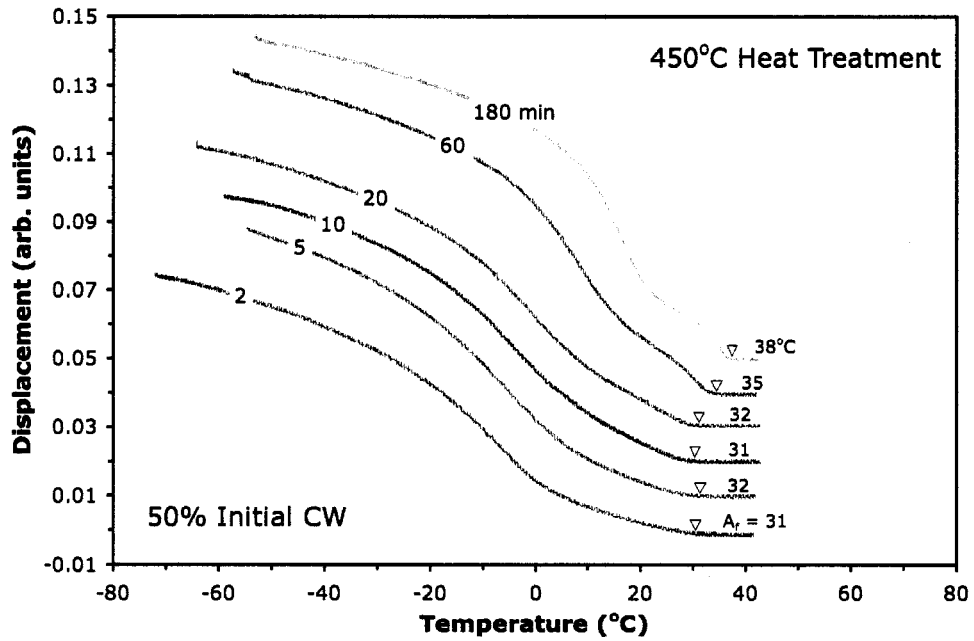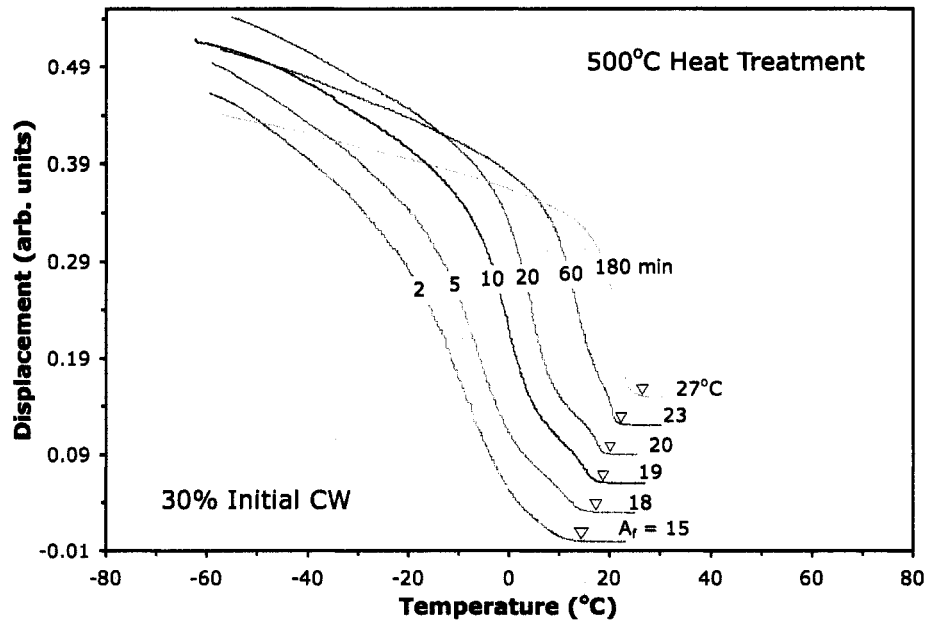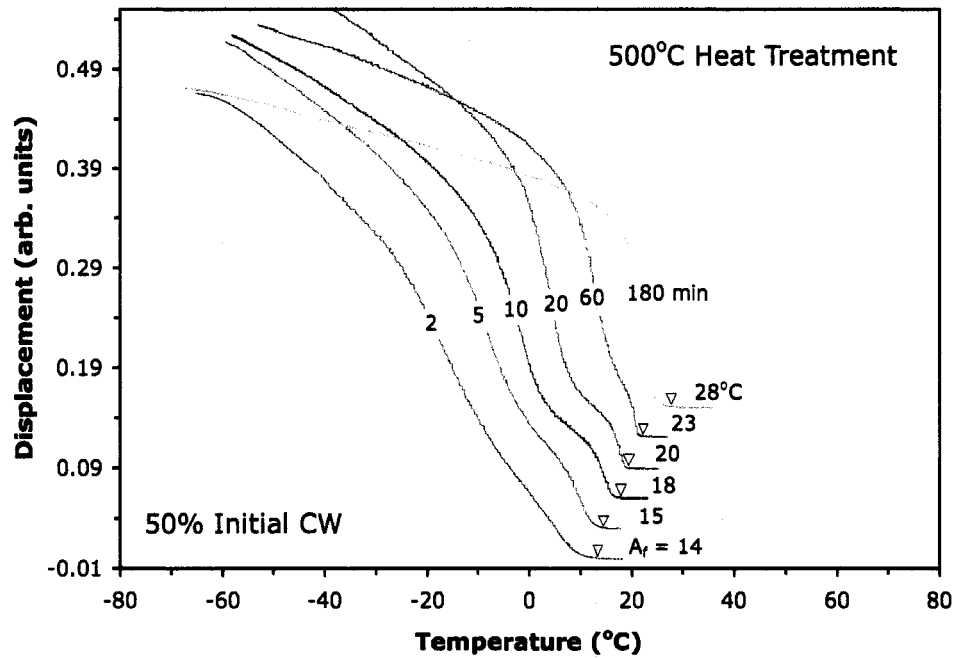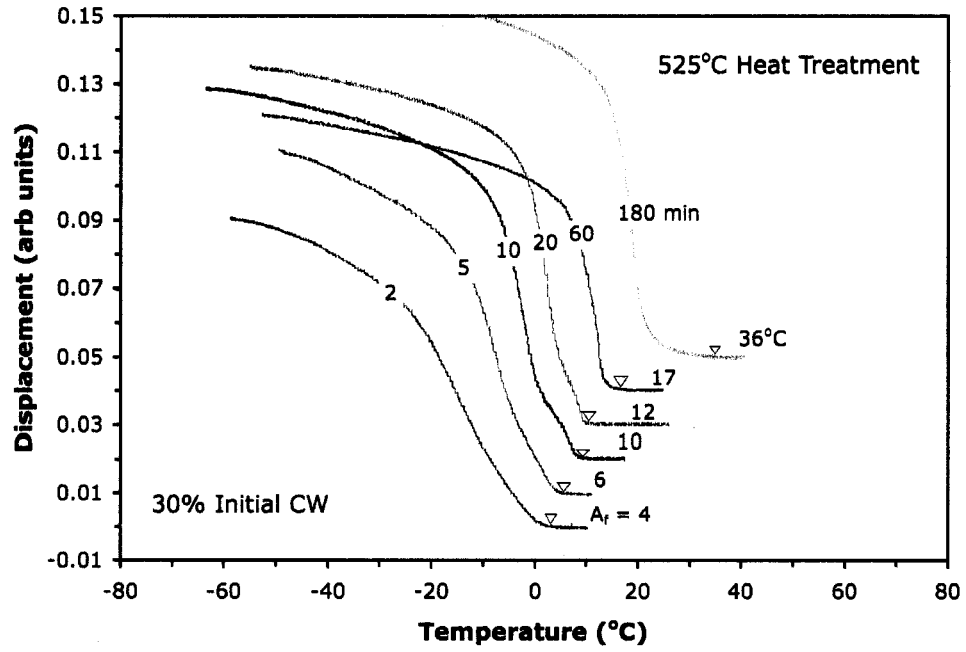
81

Figure A-5. BFR plots of 30% cold-worked wire after 450°C heat treatments.

Figure A-6. BFR plots of 50% cold-worked wire after 450°C heat treatments.

Figure A-7. BFR plots of 30% cold-worked wire after 500°C heat treatments.

Figure A-8. BFR plots of 50% cold-worked wire after 500°C heat treatments.

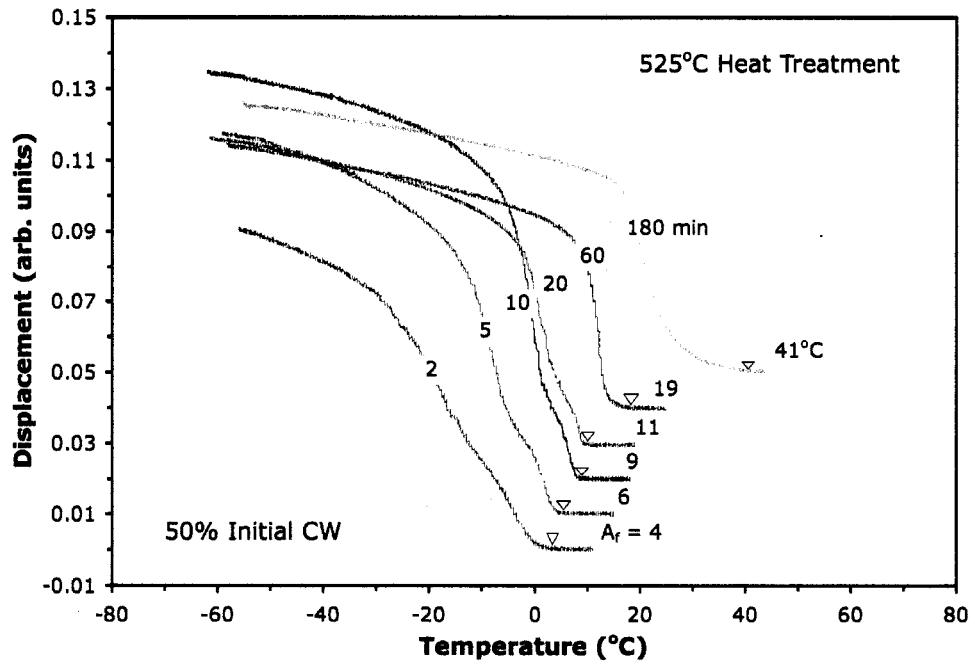Figure A-9. BFR plots of 30% cold-worked wire after 525°C heat treatments.

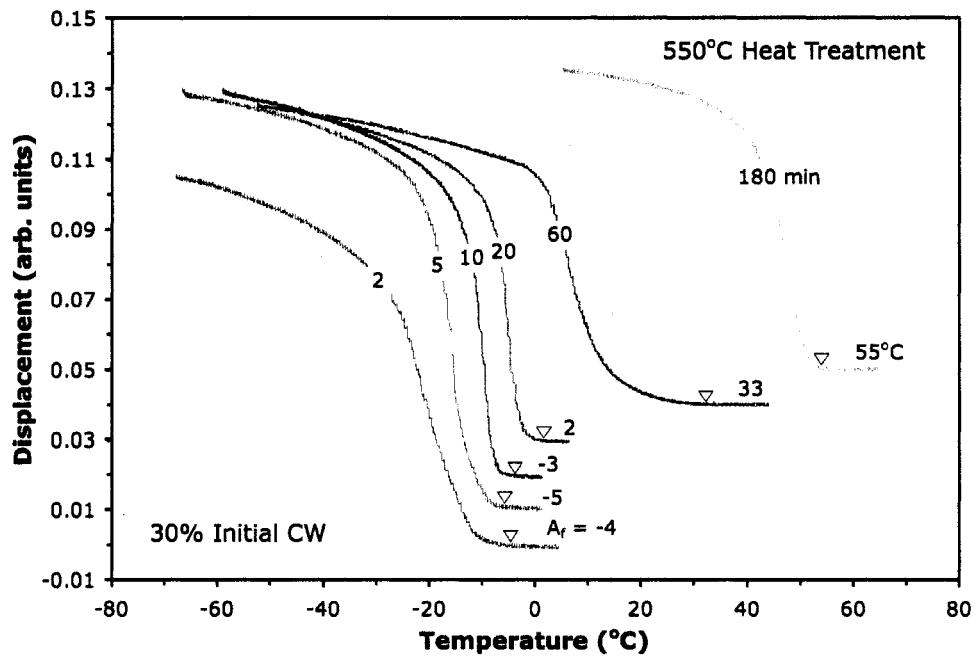Figure A-10. BFR plots of 50% cold-worked wire after 525°C heat treatments.

Figure A-11. BFR plots of 30% cold-worked wire after 550°C heat treatments.
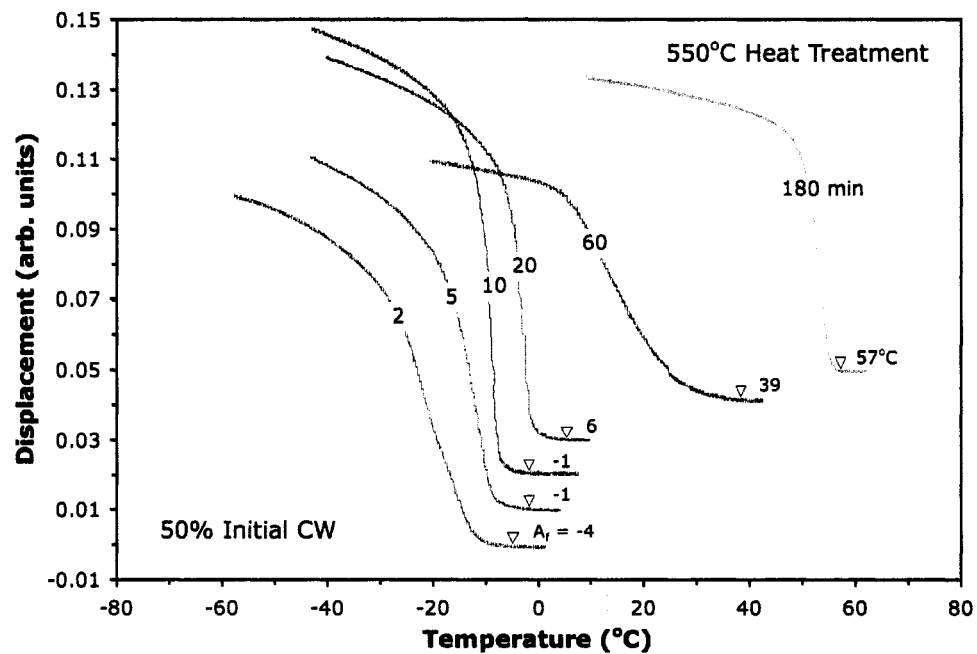

Figure A-12. BFR plots of 50% cold-worked wire after 550°C heat treatments.

85

Spectrum processing :
Peak possibly omitted : 3.735 keV

Processing option : All elements analyzed (Normalised)
Number of iterations = 2

Standard :
Ti   Ti   1-Jun-1999 12:00 AM
Ni   Ni   1-Jun-1999 12:00 AM

Element	App Conc.	Intensity Corrn.	Weight%	Weight% Sigma
Ti K	40.23	0.9818	44.46	0.57
Ni K	49.32	0.9636	55.54	0.57
Totals			100.00	

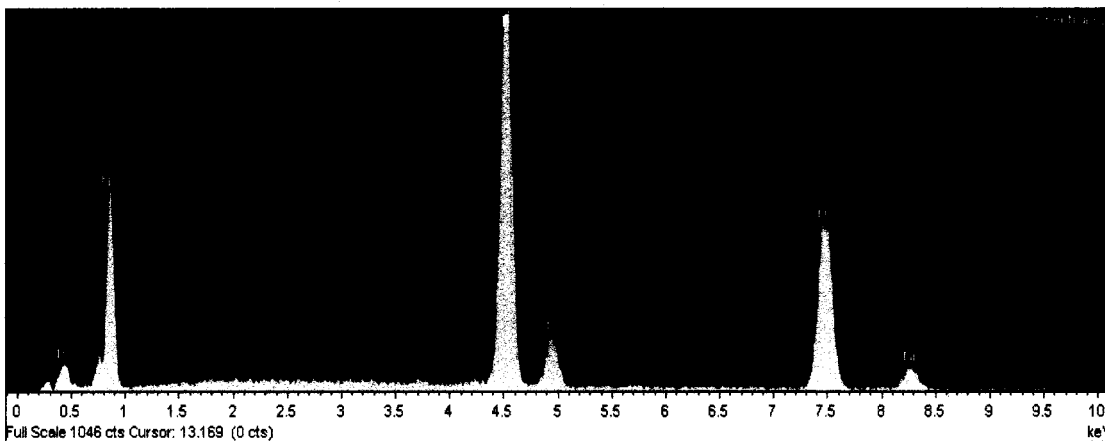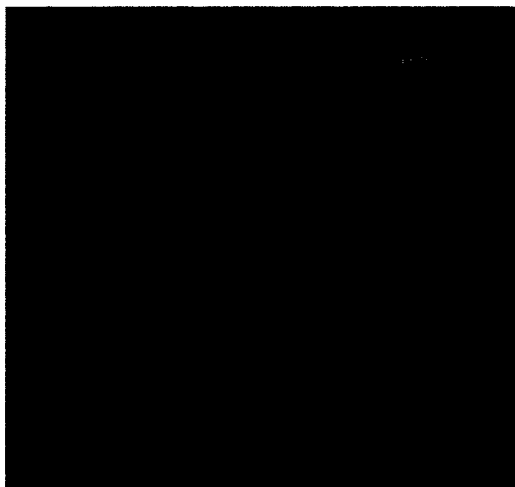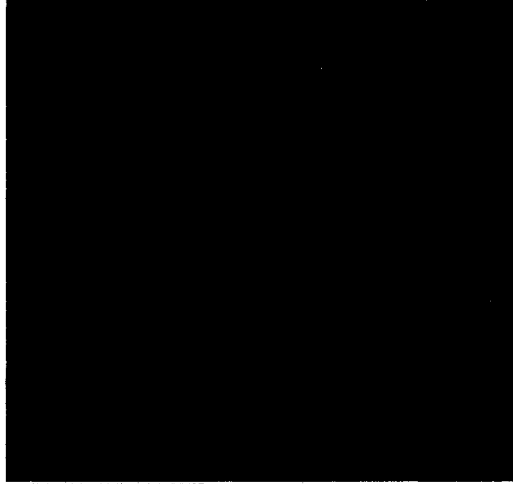Figure B-1. SEM image and accompanying EDS analysis of matrix.

86

Spectrum processing :
No peaks omitted

Processing option : All elements analyzed (Normalised)
Number of iterations = 2

Standard :
Ti   Ti   1-Jun-1999 12:00 AM
Ni   Ni   1-Jun-1999 12:00 AM

Element	App Conc.	Intensity Corrn.	Weight%	Weight% Sigma
Ti K	38.93	0.9816	43.36	0.57
Ni K	49.97	0.9645	56.64	0.57
Totals			100.00	

10μm   Electron Image 1

Full Scale 1082 cts Cursor: 13.169 (0 cts)   keV
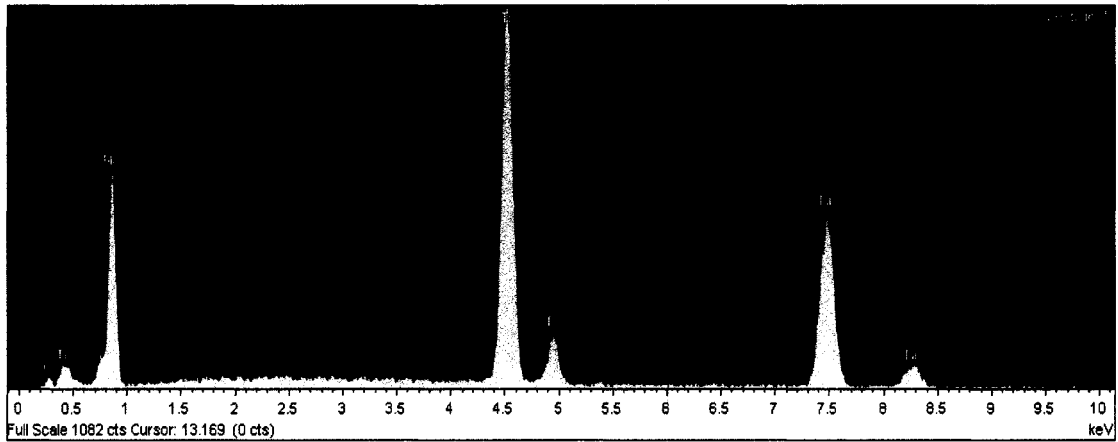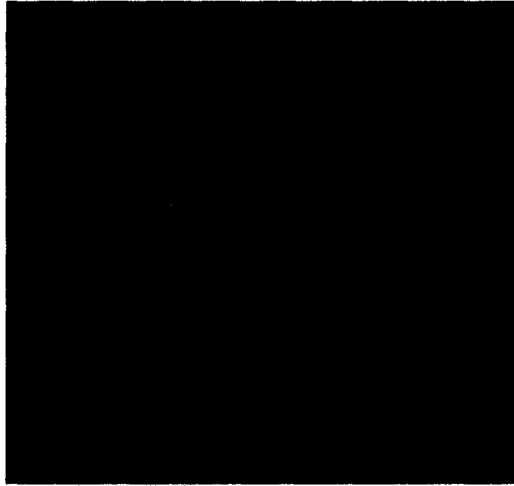
Figure B-2. SEM image and accompanying EDS analysis of precipitate.

Spectrum processing :
No peaks omitted

Processing option : All elements analyzed (Normalised)
Number of iterations = 3

Standard :
O   SiO2   1-Jun-1999 12:00 AM
Ti   Ti   1-Jun-1999 12:00 AM
Ni   Ni   1-Jun-1999 12:00 AM

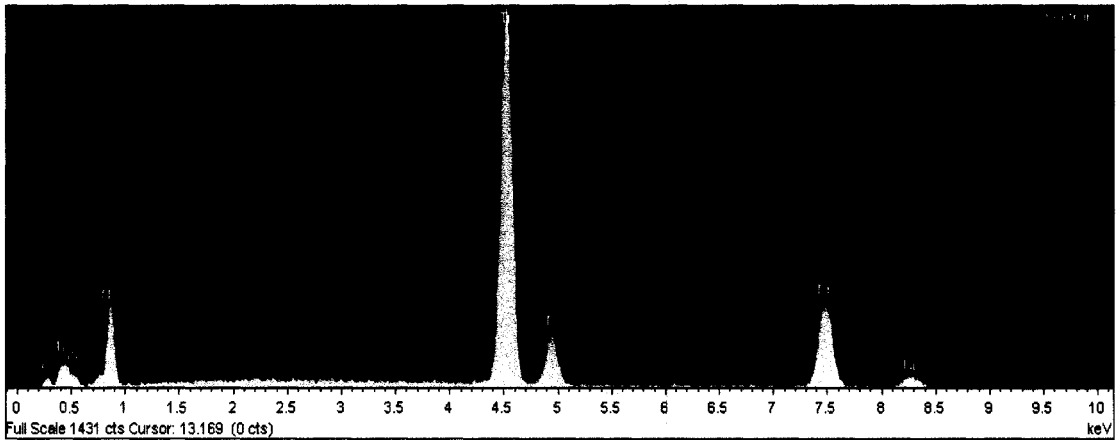| Element	App Conc.	Intensity Corrn.	Weight%	Weight% Sigma
O K	1.71	0.3052	5.96	1.41
Ti K	52.68	0.9749	57.43	1.04
Ni K	32.38	0.9401	36.62	0.82
Totals			100.00	

Figure B-3. SEM image and accompanying EDS analysis of oxide particle.